Front. Mech. Eng. 2018, 13(2): 179–210
https://doi.org/10.1007/s11465-018-0464-3

REVIEW ARTICLE

Jianyong YAO

Model-based nonlinear control of hydraulic servo systems: Challenges, developments and perspectives

Abstract Hydraulic servo system plays a significant role in industries, and usually acts as a core point in control and power transmission. Although linear theory-based control methods have been well established, advanced controller design methods for hydraulic servo system to achieve high performance is still an unending pursuit along with the development of modern industry. Essential nonlinearity is a unique feature and makes model-based nonlinear control more attractive, due to benefit from prior knowledge of the servo valve controlled hydraulic system. In this paper, a discussion for challenges in model-based nonlinear control, latest developments and brief perspectives of hydraulic servo systems are presented: Modelling uncertainty in hydraulic system is a major challenge, which includes parametric uncertainty and time-varying disturbance; some specific requirements also arise ad hoc difficulties such as nonlinear friction during low velocity tracking, severe disturbance, periodic disturbance, etc.; to handle various challenges, nonlinear solutions including parameter adaptation, nonlinear robust control, state and disturbance observation, backstepping design and so on, are proposed and integrated, theoretical analysis and lots of applications reveal their powerful capability to solve pertinent problems; and at the end, some perspectives and associated research topics (measurement noise, constraints, inner valve dynamics, input nonlinearity, etc.) in nonlinear hydraulic servo control are briefly explored and discussed.

Keywords hydraulic servo system, adaptive control, robust control, nonlinear friction, disturbance compensation, repetitive control, noise alleviation, constraint control

Received March 23, 2017; accepted May 31, 2017

Jianyong YAO (✉)
School of Mechanical Engineering, Nanjing University of Science and Technology, Nanjing 210094, China
E-mail: jerryyao.buaa@gmail.com

1 Technique background

Hydraulic servo system has been widely employed in various industrial applications by utilizing the superiorities of its large power-to-weight ratio and capability to generate large force/torque, and its controller design determines the final performance. To design an effective controller, a priori modelling of the control plant is very useful even if the final controller does not rely on the precise model information, e.g., linear proportional-integral-derivative (PID) controller. Actually, the perfect PID controller gains have strong relationship with the dynamic structure characteristics and parameters of the controlled plant.

A detailed description of the modelling of hydraulic control system has been made in Ref. [1]. In addition, by using the linearized hydraulic system model, the transfer function based control methods have also been discussed therein. Afterwards, various linear controllers, especially the PID-based controllers, are successfully and widely applied in numerous applications. However, traditional linear controllers have become difficult to meet the increasingly strict performance requirements. Moreover, inherent nonlinear features and modelling uncertainties in hydraulic systems show great challenge to the linear controllers. Hence, there is a pressing need of nonlinear based control to handle nonlinear behaviors and modelling uncertainties, and achieve more attractive control performance for high-end equipments and/or tasks in extreme environment.

The nonlinear features of hydraulic system include nonlinear pressure-flow characteristic of servo valve, saturation, dead-zone and hysteresis of servo valve, nonlinear friction in hydraulic actuators, backlash nonlinearity of mechanical connection, mechanism nonlinearity, etc. In these nonlinearities, pressure-flow nonlinearity is the most common as well as important nonlinear characteristic affecting the control performance. Essential nonlinearities highly prompt the development of model-based hydraulic nonlinear servo control theories and techniques. The core idea in this type of control method

is that firstly building the system nonlinear model in the state-space, cancelling all nonlinearities via full state feedback, and then transforming the nonlinear system dynamics to linear tracking error dynamics, finally designing linear/nonlinear feedback control laws to stabilize the system, and expecting high control performance. However, this design procedure has an extremely critical problem, that is the modelling uncertainty issue, which may deteriorate the control performance and even lead to instability. Hence, how to handle all modelling uncertainties to ensure the successful cancellation effect of nonlinearities is the key to the success of this kind of design concept.

For hydraulic servo systems, the modelling uncertainties include parametric uncertainties and uncertain nonlinearities [2]. Parametric uncertainties include the unknown driven mass load, friction coefficients which can be explicitly modeled, and the hydraulic parameters (e.g., effective bulk modulus, internal leakage coefficient, electrical gains of servo valve). Parametric uncertainties have the unique features that the structure of this type uncertainty is known, the value of the associated parameter is unknown but constant or slowly changing and can be thought as constant. Other general uncertainties, such as unmodeled friction behaviors, complicated leakage features and external disturbances, are called uncertain nonlinearities or time-varying disturbances.

Nonlinear adaptive backstepping control techniques [3], which can estimate the unknown parameters online, are effective to handle parametric uncertainties. Therefore, various adaptive based control schemes have been proposed for hydraulic systems. However, the uncertain nonlinearities (e.g., nonlinear frictions and external disturbances) are neglected and only the parametric uncertainties are taken into consideration in traditional adaptive controller design. As a matter of fact, it is impossible to obtain the accurate mathematical model of practical hydraulic system since there always exist some complicated effects that cannot be modeled by explicit functions. Hence, the uncertain nonlinearities always exist in hydraulic systems and restrict the control performance improvements.

Nonlinear robust control techniques have also been utilized for hydraulic servo systems in some occasions. This kind of control method has some robustness with respect to both parametric uncertainties and uncertain nonlinearities. However, typical Nonlinear robust control handle parametric uncertainties in a conservative way, i.e., using the nominal values of the unknown parameters, and lumping the parameter deviation effects into generalized disturbances. With the assumption that all generalized disturbance is bounded, linear/nonlinear robust feedback law can be designed, but the nonlinear robust controller can only ensure the tracking error is bounded and the high precision tracking is achieved by employing large feedback gains in these robust controllers.

As analysed above, hydraulic servo systems both exist parametric uncertainty and uncertain nonlinearity. Hence, how to handle modelling uncertainties by merging adaptive control, nonlinear robust control, disturbance observer technique, etc., is more attractive and useful in practice. In this paper, the modelling and control challenges are analyzed firstly, and some recent developments of nonlinear-model-based hydraulic servo control proposed by the author and his team are reviewed, after that some perspectives are made of opening problems.

2 Nonlinear model and challenges of hydraulic servo system

2.1 Physical model

The servo-valve controlled hydraulic actuator is considered in this paper. It contains two physical types, i.e., double-rod hydraulic cylinder illustrated in Fig. 1(a) and bidirectional hydraulic motor in Fig. 1(b). They have the same architecture, and the modelling, control methods are interchangeable. In the following, the valve-controlled bidirectional hydraulic motor is taken as an example to develop the nonlinear physical model.

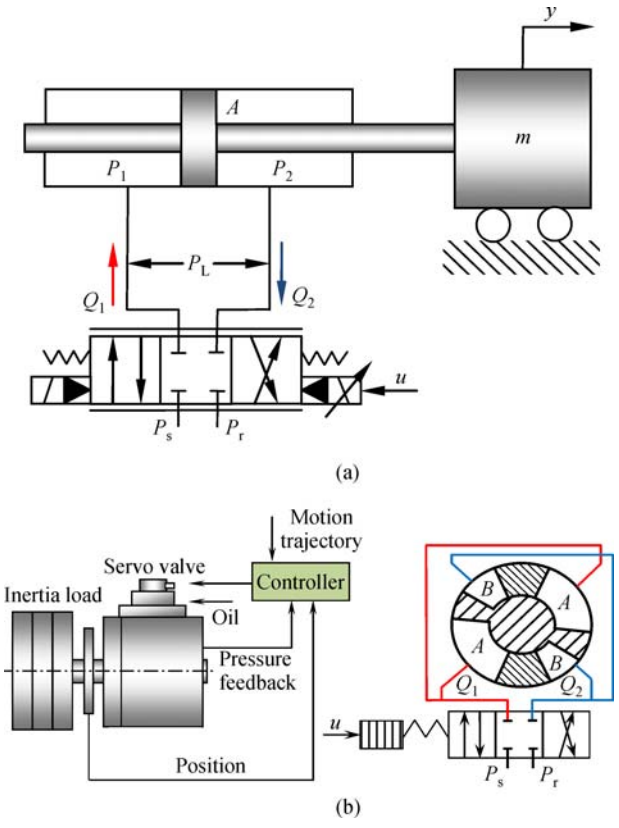

Fig. 1 The schematic diagram of the hydraulic servo system. (a) Servo-valve controlled double rod hydraulic cylinder; (b) servo-valve controlled bidirectional hydraulic motor

As shown in Fig. 1(b), an inertia load is driven by a servo-valve controlled bidirectional hydraulic motor whose structure is depicted in the right of Fig. 1(b). In the hydraulic control system, the supply pressure P_s is invariable, which is guaranteed by a relief valve and accumulator. The return pressure P_r is small since it is directly connected to the oil tank. The goal is to have the inertia load to track any smooth motion trajectory as closely as possible. The torque balance equation of the inertia load is

$$m\ddot{y} = P_L A - f(t), \tag{1}$$

where m is the moment of inertia of the load, y is the angular displacement of the load, $P_L = P_1 - P_2$ is the load pressure in which P_1 and P_2 are pressures inside the two chambers of the actuator, A denotes the radian displacement of the actuator and $f(t) = f_r(t) + f_e(t)$ in which $f_r(t)$ denotes the modeled friction effects and $f_e(t)$ denotes other unmodeled disturbances. Various friction models have been proposed in Ref. [4], and they typically contain discontinuous signum function to describe the switching effect at zero velocity point. However, non-differentiable friction model cannot be used in backstepping design, and hence is not suitable for hydraulic servo control. The following smooth friction models have been widely utilized in model-based hydraulic servo control:

$$f_r(t) = B\dot{y}, \tag{2}$$

or

$$f_r(t) = B\dot{y} + A_f S_f(\dot{y}), \tag{3}$$

where B is viscous friction coefficient, $A_f S_f$ is the approximated nonlinear Coulomb friction in which A_f is the amplitude and S_f is a known continuous shape function.

It is worth noting that although various dynamic friction models have been proposed in Refs. [5,6], they are non-differentiable due to containing discontinuous sign function. That is why most nonlinear hydraulic control methods do not employ them to complete friction compensation.

Considering the compressibility of oil, the pressure dynamics inside the two chambers can be given by [1]

$$\begin{cases} \dot{P}_1 = \dfrac{\beta_e}{V_1}[-A\dot{y} - q_L(P_L) + q_1(t) + Q_1] \\ \dot{P}_2 = \dfrac{\beta_e}{V_2}[A\dot{y} + q_L(P_L) - q_2(t) - Q_2] \end{cases}, \tag{4}$$

where $V_1 = V_{01} + Ay$, $V_2 = V_{02} - Ay$ are the control volumes of the two chambers of the actuator in which V_{01} and V_{02} are the initial control volumes, β_e is the effective oil bulk modulus, q_L is the total internal leakage of the actuator which is related to P_L, $q_1(t)$ and $q_2(t)$ are the unmodeled errors, Q_1 is the supplied flow rate to the forward chamber, and Q_2 is the return flow rate of the return chamber. Since a servo valve is utilized in this paper, its dynamics are neglected in comparison to our interest frequency rang due to the much faster valve response. Thus, it can be assumed that the control input voltage u is proportional to the spool valve displacement x_v. Then, Q_1 and Q_2 can be expressed as

$$\begin{cases} Q_1 = k_t u[s(u)\sqrt{P_s - P_1} + s(-u)\sqrt{P_1 - P_r}] \\ Q_2 = k_t u[s(u)\sqrt{P_2 - P_r} + s(-u)\sqrt{P_s - P_2}] \end{cases}, \tag{5}$$

where k_t is the total flow gain and the definition of the function $s(u)$ is

$$s(u) = \begin{cases} 1, & \text{if } u \geqslant 0 \\ 0, & \text{if } u < 0 \end{cases}. \tag{6}$$

Remark 1: In the pressure dynamic model Eq. (4), potential external leakage is not explicitly expressed, and its effects can be lumped into modelling errors, i.e., $q_1(t)$ and $q_2(t)$. In addition, the internal leakage $q_L(P_L)$ is typically modeled as proportional to the load pressure P_L, i.e., $q_L(P_L) = C_t P_L$, where C_t is the internal leakage coefficient of the actuator. This model might be not precise for different actuators, see an example in Refs. [7,8]. The other effects of internal leakage can also be lumped into $q_1(t)$ and $q_2(t)$.

Besides Eqs. (4) and (5) describing the effects of nonlinear pressure-flow characteristic of the servo valve, there still exists a simplified nonlinear model with the help of the load flow concept, the derivation can be found in Ref. [1], in this case, the load pressure dynamics is

$$\frac{V_t}{4\beta_e}\dot{P}_L = -A\dot{y} - C_t P_L + Q_o + Q(t) + Q_L, \tag{7}$$

where $V_t = V_1 + V_2$ is the total control volume of the actuator, $Q(t)$ is the modelling error caused by complicated internal leakage, external leakage, etc., and $Q_L = (Q_1 + Q_2)/2$ is the load flow. The relationship between Q_L and the spool valve displacement x_v is [1]

$$Q_L = k_q x_v \sqrt{P_s - \text{sign}(x_v) P_L}, \tag{8}$$

where $k_q = C_d w\sqrt{1/\rho}$ is the flow gain and sign(x_v) is

$$\text{sign}(x_v) = \begin{cases} 1, & \text{if } x_v \geqslant 0 \\ -1, & \text{if } x_v < 0 \end{cases}, \tag{9}$$

where C_d is the discharge coefficient, w is the spool valve area gradient, and ρ is the oil density.

As discussed above, the relationship between x_v and u can be approximated as $x_v = k_i u$, where $k_i > 0$ is an electrical gain. Therefore, Eq. (8) can be written as

$$Q_L = k_t u\sqrt{P_s - \text{sign}(u) P_L}, \tag{10}$$

where $k_t = k_q k_i$ is the total flow gain.

The model Eqs. (7)–(10) can be utilized in the case that

only pressure sensor is mounted on the system, that is to say, the information of P_1 and P_2 cannot be measured and hence nonlinear feature defined by Eq. (5) cannot be utilized in controller design. There is another case for controller design by using Eqs. (7)–(10), i.e., the estimation/observation of load pressure signal P_L only via position information, this case will be discussed later.

2.2 State-space model

Model-based nonlinear control for hydraulic systems is typically developed from the state-space model, hence a suitable state-space model is a favorable start-point for hydraulic nonlinear control. However, there is no strict rule about how to choose state variables, as long as the dynamics of the chosen state variables could sufficiently and necessarily describe the original system dynamics. The following provides two common state-space models.

2.2.1 Load pressure based state-space model

From the physical model Eqs. (1), (4) and (5), it is known that the state variables of the considered hydraulic system include y, $\dot{y}$, P_1, and P_2. However, only y, $\dot{y}$, and P_L are necessary to control in practice. Hence, the state variables can be defined as $\boldsymbol{x}=[x_1, x_2, x_3]^T=[y, \dot{y}, P_L]^T$, then the state equation describing the whole system can be written as

$$\begin{cases} \dot{x}_1 = x_2 \\ \dot{x}_2 = \dfrac{1}{m}[Ax_3 - f_r(t) - f_e(t)] \\ \dot{x}_3 = \beta_e k_t\left(\dfrac{R_1}{V_1}+\dfrac{R_2}{V_2}\right)u - \beta_e\left(\dfrac{1}{V_1}+\dfrac{1}{V_2}\right)(Ax_2 + C_t x_3) \\ \qquad + q(t) \end{cases}, \tag{11}$$

where

$$\begin{cases} R_1 = s(u)\sqrt{P_s - P_1} + s(-u)\sqrt{P_1 - P_r} \\ R_2 = s(u)\sqrt{P_2 - P_r} + s(-u)\sqrt{P_s - P_2} \\ q(t) = \beta_e\left[\dfrac{q_1(t)}{V_1}+\dfrac{q_2(t)}{V_2}\right] \end{cases}. \tag{12}$$

In Eq. (11), a reduced-order state-space model is built, and based on this model, various nonlinear controllers could be developed to stabilize the system Eq. (11) and achieve advanced tracking performance based on the model above. By the way, the system Eq. (11) is based on the pressure dynamics in Eqs. (4) and (5), it can also be developed from Eqs. (7)–(10), in which the load flow concept is utilized. No matter whatever the case, it is worth noting that there exists a zero dynamic problem since the final controller can only ensure the boundedness of the state variables, i.e., the developed controller can ensure the signal P_L is bounded, however, the boundedness of the original state variables P_1, P_2 is still remained in theory level. The boundedness of P_L cannot ensure the boundedness of P_1 and P_2. To complete the theoretical analysis, singular value perturbation theory is suggested to help analyzing the boundedness of P_1 and P_2. In practice, from the viewpoint of engineering, it can be deduced that the inside pressure P_1 and P_2 are almost always no more than the supply pressure, hence, a practical assumption can be made for the built state-space model, and this assumption has been widely employed in model-based nonlinear control for hydraulic systems.

Assumption 1: In normal working conditions, P_1 and P_2 are both bounded by P_r and P_s, i.e., $0 < P_r < P_1 < P_s$, $0 < P_r < P_2 < P_s$.

2.2.2 Acceleration-based state-space model

Besides the load pressure based state-space model, there also exists acceleration based state-space model, and this model is typical utilized for special control purpose, such as velocity and acceleration constraint control, reduction of unmatched disturbance. As discussed in Ref. [2]. it is reasonable to assume the unmodeled term $f_e(t)$ is continuously differentiable, then based on the dynamics in Eqs. (1) and (2), combining the pressure dynamics in Eqs. (7)–(10), the state variables can be defined as $\boldsymbol{x}=[x_1, x_2, x_3]^T=[y,\dot{y},\ddot{y}]^T$, thus the state equation to describe the whole system can be written as [8]

$$\begin{cases} \dot{x}_1 = x_2 \\ \dot{x}_2 = x_3 \\ \dfrac{mV_t}{4A\beta_e k_t}\dot{x}_3 = U - \left(\dfrac{A}{k_t}+\dfrac{C_t B}{Ak_t}\right)x_2 \\ \qquad\qquad - \left(\dfrac{C_t m}{Ak_t}+\dfrac{V_t B}{4A\beta_e k_t}\right)x_3 - \Delta(t) \end{cases}, \tag{13}$$

where

$$U \triangleq u\sqrt{P_s - \mathrm{sign}(u)P_L},$$

$$\Delta(t) \triangleq \frac{1}{k_t}q(t) + \frac{C_t}{Ak_t}f_e(t) + \frac{V_t}{4A\beta_e k_t}\dot{f}_e(t). \tag{14}$$

Remark 2: In Eq. (14), a new variable U is defined to represent the control input to the system. Since pressure sensors have been mounted in our system, i.e., $(P_s - \mathrm{sign}(u)P_L)^{1/2}$ can be calculated in real-time, only if U is determined, then u can be calculated by $U/(P_s - \mathrm{sign}(u)P_L)^{1/2}$. Hence, the design mission is to achieve high tracking performance by synthesizing a suitable signal U.

2.3 Control challenges

As pointed out in technique background, the hydraulic

system exists lots of modelling uncertainties, and these uncertainties are the main obstacles of developing model-based nonlinear controllers for hydraulic systems. Although there are lots of advanced nonlinear control theories, such as adaptive control, sliding model control, observer, they maybe not directly suitable for hydraulic servo control, due to the specific characteristics of valve-controlled hydraulic system. The control challenges are reflected in

1) Unlike other mechatronic servo systems, such as servo motor, hydraulic system exists heavy parametric uncertainty and uncertain nonlinearity. The hydraulic parameters, such as the internal leakage, the effective bulk modules, are very sensitive to temperature, air/water pollution and/or component wear, etc. The typical system parameters, such as m, B, A_f, β_e, C_t, k_t, may be all possible to be unknown. Besides, one of the uncertain nonlinearity, the large external disturbance may be not avoided in practice, since the main task of hydraulic actuator is to drive heavy external disturbances for some hydraulic applications, such as aircraft actuator is to overcome aerodynamic force, hydraulic machine tool is to overcome cutting force during manufacturing; friction is also a main source of uncertain nonlinearity, considering the sealing effect, the friction force is very difficult to reduce for hydraulic actuators. The friction force and the internal leakage are a couple of contradictions: small friction usually means large internal leakage, and vice versa. As pointed out in Ref. [9], the friction force can reach 30% of the total output torque of the hydraulic actuator in some cases. Another difficulty for friction is that it is very hard to precisely model it. Although there are lots of friction models in literature, the exact model for nonlinear friction is still debatable. The modelling complexity of friction is an intractable problem, more complex to model the friction, more precise to describe the nonlinear feature, however, more difficult to be utilized in controller design, and vice versa. The third source of the uncertain nonlinearity is the unmodeled uncertainty in pressure dynamics, the internal leakage and external leakage are very difficult to be exactly described, in addition, the nonlinear pressure-flow feature of servo valve is also an approximation, there are lots of turbulent flow effects near valve orifice. Overall, uncertain nonlinearity indeed exists in hydraulic systems and typically cannot be ignored.

2) The hydraulic system exists complex input nonlinearity. No matter what the type of flow equation is utilized, it possesses complex input nonlinearity. From Eqs. (5) and (10), it can be found that the control input voltage u times a nonlinear term which contains u again, i.e., $uf(\cdot, u)$, $f(\cdot, u)$ is a nonlinear function with respect to u. From this point, it is clear that the controlled nonlinear system is non-affine. Non-affine feature makes lots of nonlinear control theories and methods not suitable for hydraulic systems. Current nonlinear control methods for non-affine systems are very complex and difficult in implementation in common, and these methods still stay at the theoretical level. In practice, to develop model-based nonlinear control methods for hydraulic system, the researchers usually ignore the non-affine effects, and deduce the final control input with a specific term over the nonlinear function $f(\cdot, u)$, just like the implementation way given in Remark 2. This practical implementation method is useful for most cases. However, if the valve-spool x_v does not proportion to control input u, at high frequency as an example, and the spool position is unavailable for measurement, then the control design will be caught in the extremity by the non-affine feature. Besides, the nonlinear effect sign(u), there are other input nonlinearities, such as dead-zone effect of valve spool, saturation and hysteresis, these nonlinear effects will be coupled with the nonlinear function sign(u), and makes the control problem more intractable and difficult.

3) Hydraulic systems typically exist mismatched uncertainty. The so-called mismatched uncertainty can be comprehended as the uncertainty that does not appear in the dynamic channel with the final control input u. More concrete for hydraulic system, see the system model Eq. (11), all possible uncertainties in the second dynamic equation are mismatched uncertainties, i.e., the unknown case for m, A, $f_r(t)$ and $f_e(t)$. The mismatched uncertainty will cause the control problem more inconvenient, since the final control u cannot be designed to handle these unmatched uncertainties directly. To complete the control mission with mismatched uncertainty, backstepping design has to be employed. Although backstepping design can help greatly coping with mismatched uncertainty, its unique feature may bring other troubles for controller design in some ad hoc cases, e.g., differential explosion issue. Although there exist available methods to alleviate the difficulty in differential explosion, such as dynamic surface control [10,11], command filtered backstepping [12,13], their controller design and stability analysis are more complex and difficulty. Usually, only one-step backstepping is suitable for hydraulic systems. This is one reason why servo-valve dynamics are ignored in most literatures. If one-order, or second-order servo-valve dynamics are taken into consideration, the whole order of the considered hydraulic system model will increase, and the mismatched uncertainty will become deep from the final control input u, then differential explosion issue is inevitable. Besides differential explosion in backstepping, mismatched uncertainty will cause other practical problems when considering other control purpose, such as state constraints, sliding mode concept design, observer design. Hence, in some cases, the system model Eq. (13) with the help of acceleration information is more welcome, since this model does not exist mismatched uncertainty, and can bring some convenience to controller design. However, it has also to be admitted the system model

Eq. (13) typically requires acceleration feedback for full state feedback based controller design, which is not easy or common in practice.

4) Besides above common control challenges, specific control missions may cause more challenges, for example, exact and uncomplicated nonlinear friction compensation for low velocity tracking, more tracking accuracy requirements for repetitive tasks, output feedback tracking control in the case that the system cost/weight/volume is limited, output velocity/acceleration constraint requirement with tracking control, etc. During the following controller designs, it will be discussed some ad hoc control challenges in detail when it suffered.

3 Model-based nonlinear control

Model-based nonlinear control is a powerful tool to handle the nonlinearities in hydraulic systems, the problem is how to handle various modelling uncertainties. As discussed above, the uncertainty in hydraulic systems includes parametric uncertainty and uncertain nonlinearity. Based on the different uncertainty circumstances, the author will discuss the model-based nonlinear control techniques in the following cases:

Case 1: The considered hydraulic system possesses simple structure, and its load structure is unitary and known. Moreover, all system parameters can be precisely identified, and their variations are not sensitive to the working environment, or the whole run of the system is in a very short time, and hence assuming the system parameters are constant and known is acceptable. In summary, the hydraulic system can be ideally and precisely modeled, and the model exists little uncertainty, only nonlinearity hampers the development of the high-performance controller. In this case, feedback linearization control is recommended, and high tracking performance can be expected.

Case 2: A common case for hydraulic system is that the system exists parametric uncertainties, i.e., the load parameters and hydraulic parameters are unknown, m, B, A_f, β_e, C_t, and k_t are unknown. However, the system does not exist uncertain nonlinearities. In summary, the hydraulic system can be structurally modeled, and the model only exists parametric uncertainty which along with nonlinearity and hampers the development of the high-performance controller. In this case, nonlinear adaptive control is recommended, and adaptive law can be synthesized to result in high tracking performance. The traditional adaptive control can easily handle the parameters appearing in the system in a linear way, i.e., the parameters m, B, A_f, β_e, C_t, and k_t. However, there are still some parameters such as V_{01}, V_{02}, P_s, and P_r, they appear in the system via a nonlinear way, and if they are unknown, to online estimate them by developing an adaptive law is challenging, some possible solutions with this nonlinear parameter adaptation can be found in Refs. [14–16].

Case 3: Another common case for hydraulic system is that the system exists uncertain nonlinearities, i.e., the systems are disturbed by unknown and time-varying functions, e.g., $f_e(t)$, $q(t)$ in Eq. (11) and $\Delta(t)$ in Eq. (13). All system parameters are exactly known or their nominal values can be utilized and the deviation effects with the nominal values can be lumped into time varying disturbances. With some suitable assumptions, such as the boundedness of various time varying disturbances, nonlinear robust controller can be developed along with the system nonlinearity to enhance the robustness against disturbances and improve the tracking performance.

Case 4: A more common case for hydraulic system is that the system both exists parametric uncertainty and uncertain nonlinearity, as discussed in the control challenges. The coupling effect between the parametric uncertainty and uncertain nonlinearity make the development of nonlinear advanced controller for hydraulic system more challengeable. In this area, various combinations of adaptive and robust control methods have been proposed with the expectation that the parameter uncertainty can be reduced by adaptive law and the uncertain nonlinearity could be suppressed by nonlinear robust law.

Case 5: With a suitable assumption that the uncertain nonlinearity is smooth, an enhanced robust mechanism is developed by the author and his co-operators. The enhanced robust control law combines a robust integral of the sign of the error (RISE) controller which can asymptotically compensate smooth disturbances, and typically asymptotic tracking performance can be achieved.

Case 6: The hydraulic system may execute some specific tasks, for example, repetitive tasks. Although the system both exists parametric uncertainty and uncertain nonlinearity, in repetitive tasks, all closed-loop system signals approximately appear periodicity, and no doubt the state-dependent disturbances will possess some periodicity. This feature provides us an opportunity to precisely compensate these disturbances via adaptive mechanism, i.e., developing an adaptive repetitive controller.

Case 7: Low velocity tracking performance is an important capability for hydraulic systems, especially for the hydraulic test equipments. In fact, friction can lead to undesired stick-slip motion and limit cycles. How to appropriately model and compensate friction is a hotspot in mechanical low velocity tracking. Nonlinear friction contains various friction actions, such as stiction friction, Coulomb friction, and Stribeck effect. Since the LuGre friction model proposed in Ref. [5] can represent the majority of friction effects and is easy to be incorporated in the control design, it has been widely employed in servo control area. To handle the unmatched friction effects in hydraulic systems, backstepping design method is often utilized which requires differentiation operation on the employed nonlinear friction model. However, the draw-

back of the LuGre friction model is that it is piecewisely continuous and thus non-differentiable. Hence, this greatly limits the utilization of the LuGre friction model in hydraulic control design. How to use the LuGre friction model in backstepping controller design for hydraulic systems to compensate the friction effects and then to achieve tracking performance improvement is still a pending issue. Therefore, it is necessary to develop new continuously differentiable LuGre friction model for hydraulic system.

Case 8: As we know, almost all nonlinear approaches for hydraulic systems have used full-state feedback. It means that those controller designs need velocity and pressure signals besides position signal. However, in plenty of practical hydraulic systems, only position sensor is mounted due to some realistic restrictions such as cost and/or structure. Moreover, the measured velocity and pressure signals are usually contaminated by heavy noise which has adverse effects on the control performance of full-state feedback controllers. Thus, it is an imperious demand to develop an output feedback nonlinear control scheme which only requires the output measurement for hydraulic servo system.

Case 9: Backstepping method has been widely employed in controller design of hydraulic systems. However, the controllers designed by directly applying the standard backstepping method may be aggressive in practice. Those controllers are not recommended for practical hydraulic systems with hard constraints on the system states and control input saturation. The practical hydraulic systems, especially those testing equipments which have interaction with the environment and the unit under test (UUT), have potential risks due to their high load and stiffness properties. The UUT may be damaged by overlarge velocity and/or acceleration if their hard constraints are ignored in the control design. Hence, it is necessary to investigate the advanced nonlinear control strategy for hydraulic servo systems with consideration of both velocity and acceleration constraints.

3.1 Feedback linearization control

As described in Case 1, the mathematic model of the discussed hydraulic system in this case is known. In order to present the feedback linearization (FBL) control for a more general case, it is considered the load pressure based state-space model in Eq. (11), and the modeled friction $f_r(t)$ in Eq. (3), then the system model for this case can be given as

$$\begin{cases} \dot{x}_1 = x_2 \\ \dot{x}_2 = \dfrac{1}{m}[x_3 - Bx_2 - A_f S_f(x_2)] \\ \dot{x}_3 = \beta_e k_t \left(\dfrac{R_1}{V_1} + \dfrac{R_2}{V_2}\right) u - \beta_e \left(\dfrac{1}{V_1} + \dfrac{1}{V_2}\right)(Ax_2 + C_t x_3) \end{cases}. \tag{15}$$

Assumption 2: The desired position command $y_d = x_{1d}(t) \in C^3$ is bounded.

3.1.1 Feedback linearization controller design

A set of error variables can be defined as

$$\begin{aligned} &z_1 = x_1 - x_{1d},\ z_2 = \dot{z}_1 + k_1 z_1 = x_2 - \alpha_1, \\ &\alpha_1 \triangleq \dot{x}_{1d} - k_1 z_1,\ z_3 = x_3 - \alpha_2, \end{aligned} \tag{16}$$

where x_{1d} is desired motion trajectory and z_1 is the output tracking error, k_1 is a positive feedback gain, α_1 is the virtual control law of the state x_2, and z_2 is the discrepancy between the actual state x_2 and virtual control α_1, α_2 is the virtual control law of the state x_3, and z_3 is the discrepancy between the actual state x_3 and virtual control α_2.

Combining the defined error variables in Eq. (16) and the system model Eq. (15), the error dynamics can be expressed as

$$\begin{cases} \dot{z}_2 = \dfrac{1}{m}[A(z_3 + \alpha_2) - Bx_2 - A_f S_f(x_2)] - \dot{\alpha}_1 \\ \dot{z}_3 = \beta_e k_t \left(\dfrac{R_1}{V_1} + \dfrac{R_2}{V_2}\right) u - \beta_e \left(\dfrac{1}{V_1} + \dfrac{1}{V_2}\right)(Ax_2 + C_t x_3) - \dot{\alpha}_2 \end{cases}. \tag{17}$$

Therefore, the feedback linearization controller u and the virtual control law α_2 can be synthesized as

$$\begin{cases} u = \dfrac{1}{\beta_e k_t \left(\dfrac{R_1}{V_1} + \dfrac{R_2}{V_2}\right)} \\ \qquad \cdot \left[\beta_e \left(\dfrac{1}{V_1} + \dfrac{1}{V_2}\right)(Ax_2 + C_t x_3) + \dot{\alpha}_2 - k_3 z_3\right] \\ \alpha_2 = \dfrac{1}{A}[Bx_2 + A_f S_f(x_2) + m\dot{\alpha}_1 - k_2 z_2] \end{cases}, \tag{18}$$

where k_2 and $k_3 > 0$ are the feedback gains.

By substituting α_2 and the actual control input u into the error dynamics in Eq. (17), one obtains

$$\dot{z}_1 = z_2 - k_1 z_1,\ m\dot{z}_2 = Az_3 - k_2 z_2,\ \dot{z}_3 = -k_3 z_3. \tag{19}$$

It can be seen from Eq. (19) that the nonlinear error dynamics have been transformed into linear ones by utilizing the feedback linearization control method to cancel the nonlinear terms.

3.1.2 Stability analysis

Theorem 1: By selecting large control gains k_1, k_2, and k_3, the matrix $\mathbf{\Lambda}_1$ defined below will be positive definite, then the designed feedback linearization controller Eq. (18) guarantees that all closed-loop system signals are bounded and asymptotic tracking performance can be achieved, i.e., $z_1 \to 0$ as $t \to \infty$.

$$\boldsymbol{\Lambda}_1 = \begin{bmatrix} k_1 & -\frac{1}{2} & 0 \\ -\frac{1}{2} & k_2 & -\frac{A}{2} \\ 0 & -\frac{A}{2} & k_3 \end{bmatrix}. \tag{20}$$

Proof: Define a positive Lyapunov function $V_1(t)$:

$$V_1 = \frac{1}{2}z_1^2 + \frac{1}{2}mz_2^2 + \frac{1}{2}z_3^2. \tag{21}$$

Combining Eq. (19), the time derivative of $V_1(t)$ can be deduced as

$$\begin{aligned} \dot{V}_1 &= z_1\dot{z}_1 + mz_2\dot{z}_2 + z_3\dot{z}_3 \\ &= -k_1z_1^2 - k_2z_2^2 - k_3z_3^2 + z_1z_2 + Az_2z_3 \\ &= -\boldsymbol{Z}^{\mathrm{T}}\boldsymbol{\Lambda}_1\boldsymbol{Z}, \end{aligned} \tag{22}$$

where $\boldsymbol{Z} = [z_1, z_2, z_3]^{\mathrm{T}}$.

Noting the matrix $\boldsymbol{\Lambda}_1$ is positive definite, thus we have

$$\dot{V}_1 \leqslant -\lambda_{\min}(\boldsymbol{\Lambda}_1)(z_1^2 + z_2^2 + z_3^2) \triangleq -W_1, \tag{23}$$

where $\lambda_{\min}(\boldsymbol{\Lambda}_1)$ is the minimal eigenvalue of matrix $\boldsymbol{\Lambda}_1$. Then, on the basis of the result in Eq. (23), according to Barbalat's lemma [3], $W_1 \to 0$ as $t \to \infty$, the results in Theorem 1 can be obtained.

3.1.3 Experimental verification

To demonstrate the effectiveness of the developed FBL control method, experimental results were obtained by comparing the nonlinear feedback linearization controller association with some suitable modifications and the velocity feed-forward proportional-integral (VFPI) controller in Ref. [17]. The two controllers were tested for a cosine trajectory with the same 1° amplitude and a series of different frequencies up to 20 Hz. The main experimental results are presented as follows. Specifically, the trajectory tracking and tracking error of the two controllers for 1°-20 Hz motion are shown in Figs. 2(a) and 2(b). The tracking performance indices of the two controllers are summarized in Table 1. All the performance indices show that the developed FBL control method achieves better tracking performance than VFPI controller. The reader is referred to Ref. [17] to get more details about the experiments.

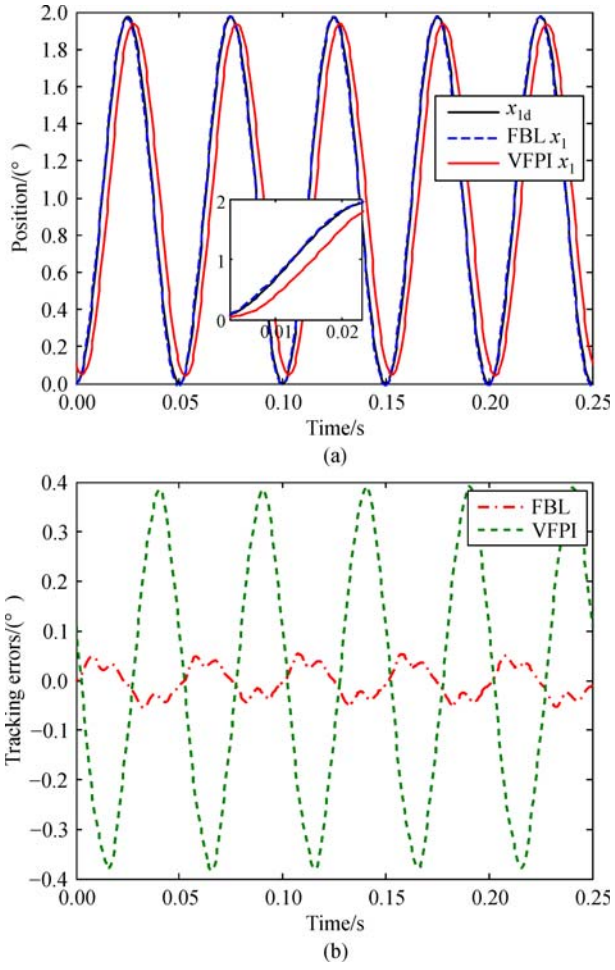

Fig. 2 Tracking performance of VFPI and FBL for 1°-20 Hz motion. (a) Trajectory tracking; (b) tracking errors of FBL and VFPI

Table 1 Performances summary with 1° amplitude testing

Frequency/Hz	Max velocity/((°) ·s^{-1})	Controller	Max error/(°)	Phase lag
5	31.4	VFPI	0.100	0.5°
5	31.4	FBL	0.030	Invisible
10	62.8	VFPI	0.200	12.2°
10	62.8	FBL	0.026	Invisible
15	94.2	VFPI	0.300	16.8°
15	94.2	FBL	0.036	Invisible
20	125.6	VFPI	0.400	22°
20	125.6	FBL	0.050	Invisible

3.2 Adaptive control

For Case 2, system parametric uncertainties are specially taken into consideration and the uncertain nonlinearities are ignored. Define the uncertain parameter set $\boldsymbol{\theta} = [\theta_1, \theta_2, \theta_3, \theta_4, \theta_5, \theta_6]^{\mathrm{T}}$, where $\theta_1 = A/m$, $\theta_2 = B/m$, $\theta_3 = A_{\mathrm{f}}/m$, $\theta_4 = \beta_{\mathrm{e}}k_{\mathrm{t}}$, $\theta_5 = \beta_{\mathrm{e}}A$, and $\theta_6 = \beta_{\mathrm{e}}c_{\mathrm{t}}$. Then the system model for this case can be given by

$$\begin{cases} \dot{x}_1 = x_2 \\ \dot{x}_2 = \theta_1 x_3 - \theta_2 x_2 - \theta_3 S_{\mathrm{f}}(x_2), \\ \dot{x}_3 = \theta_4 f_1 u - \theta_5 f_2 - \theta_6 f_3 \end{cases} \tag{24}$$

where $f_1 = (R_1/V_1 + R_2/V_2)$, $f_2 = (1/V_1 + 1/V_2)x_2$, and $f_3 = (1/V_1 + 1/V_2)x_3$.

Assumption 3: The defined parameter set $\boldsymbol{\theta}$ satisfies

$$\boldsymbol{\theta} \in \Omega_\theta \triangleq \{\boldsymbol{\theta} : \boldsymbol{\theta}_{\min} \leqslant \boldsymbol{\theta} \leqslant \boldsymbol{\theta}_{\max}\}, \tag{25}$$

where $\boldsymbol{\theta}_{\min} = [\theta_{1\min}, \theta_{2\min}, \ldots, \theta_{6\min}]^{\mathrm{T}}$, $\boldsymbol{\theta}_{\max} = [\theta_{1\max}, \theta_{2\max}, \ldots, \theta_{6\max}]^{\mathrm{T}}$ are known.

3.2.1 Adaptive controller design

Define the error variables as in Eq. (16), and note the system model Eq. (24), the error dynamics can then be described as

$$\begin{cases} \dot{z}_2 = \theta_1(z_3 + \alpha_2) - \theta_2 x_2 - \theta_3 S_{\mathrm{f}}(x_2) - \dot{\alpha}_1 \\ \dot{z}_3 = \theta_4 f_1 u - \theta_5 f_2 - \theta_6 f_3 - \dot{\alpha}_2 \end{cases}. \tag{26}$$

Based on the backstepping method, the traditional adaptive controller u and the virtual control law α_2 can be designed as

$$\begin{cases} u = \dfrac{1}{\hat{\theta}_4 f_1}(\hat{\theta}_5 f_2 + \hat{\theta}_6 f_3 + \dot{\alpha}_2 - k_3 z_3) \\ \alpha_2 = \dfrac{1}{\hat{\theta}_1}\left[\hat{\theta}_2 x_2 + \hat{\theta}_3 S_{\mathrm{f}}(x_2) + \dot{\alpha}_1 - k_2 z_2\right], \end{cases} \tag{27}$$

where $\hat{\boldsymbol{\theta}}$ is the estimate of $\boldsymbol{\theta}$, $\hat{\boldsymbol{\theta}} = \left[\hat{\theta}_1, \hat{\theta}_2, \hat{\theta}_3, \hat{\theta}_4, \hat{\theta}_5, \hat{\theta}_6\right]^{\mathrm{T}}$.

Design the parameter adaptation law for $\hat{\boldsymbol{\theta}}$ as follows:

$$\dot{\hat{\boldsymbol{\theta}}} = \boldsymbol{\Gamma}\boldsymbol{\tau},\ \boldsymbol{\tau} = \boldsymbol{\varphi}_2 z_2 + \boldsymbol{\varphi}_3 z_3, \tag{28}$$

where $\boldsymbol{\Gamma} > 0$ is a diagonal adaptation rate matrix, is the adaptation function, $\boldsymbol{\varphi}_2$ and $\boldsymbol{\varphi}_3$ are regressors of parameter adaptation, and $\boldsymbol{\varphi}_2 = [\alpha_2, -x_2, -S_{\mathrm{f}}(x_2), 0, 0, 0]^{\mathrm{T}}$, $\boldsymbol{\varphi}_3 = [0, 0, 0, f_1 u, -f_2, -f_3]^{\mathrm{T}}$.

Substituting the virtual control α_2 and the actual control input u into the error dynamics Eq. (26), that is

$$\begin{cases} \dot{z}_2 = \boldsymbol{\theta}_1 z_3 - k_2 z_2 - \tilde{\boldsymbol{\theta}}^{\mathrm{T}}\boldsymbol{\varphi}_2 \\ \dot{z}_3 = -k_3 z_3 - \tilde{\boldsymbol{\theta}}^{\mathrm{T}}\boldsymbol{\varphi}_3 \end{cases}, \tag{29}$$

where $\tilde{\boldsymbol{\theta}} = \hat{\boldsymbol{\theta}} - \boldsymbol{\theta}$ is the estimation error of the unknown parameter set $\boldsymbol{\theta}$.

3.2.2 Stability analysis

Theorem 2: Based on the adaptive law in Eq. (28), selecting large enough control gains k_1, k_2, and k_3, hence the matrix $\boldsymbol{\Lambda}_2$ defined below will be positive definite,

$$\boldsymbol{\Lambda}_2 = \begin{bmatrix} k_1 & -\dfrac{1}{2} & 0 \\ -\dfrac{1}{2} & k_2 & -\dfrac{\theta_1}{2} \\ 0 & -\dfrac{\theta_1}{2} & k_3 \end{bmatrix}, \tag{30}$$

then the designed adaptive controller Eq. (27) guarantees that all closed-loop system signals are bounded and asymptotic tracking performance can be achieved, i.e., $z_1 \to 0$ as $t \to \infty$.

Proof: Define a positive Lyapunov function $V_{\mathrm{a}}(t)$ as follows:

$$V_{\mathrm{a}} = \frac{1}{2}z_1^2 + \frac{1}{2}z_2^2 + \frac{1}{2}z_3^2 + \frac{1}{2}\tilde{\boldsymbol{\theta}}^{\mathrm{T}}\boldsymbol{\Gamma}^{-1}\tilde{\boldsymbol{\theta}}. \tag{31}$$

Combing the error dynamics in Eq. (29) and applying the adaptive law in Eq. (28), the time derivative of $V_{\mathrm{a}}(t)$ can be deduced as

$$\begin{aligned} \dot{V}_{\mathrm{a}} &= z_1\dot{z}_1 + z_2\dot{z}_2 + z_3\dot{z}_3 + \tilde{\boldsymbol{\theta}}^{\mathrm{T}}\boldsymbol{\Gamma}^{-1}\dot{\hat{\boldsymbol{\theta}}} \\ &= -k_1 z_1^2 - k_2 z_2^2 - k_3 z_3^2 + z_1 z_2 + \theta_1 z_2 z_3 \\ &= -\boldsymbol{Z}^{\mathrm{T}}\boldsymbol{\Lambda}_2\boldsymbol{Z}. \end{aligned} \tag{32}$$

Noting the matrix $\boldsymbol{\Lambda}_2$ is positive definite, thus

$$\dot{V}_{\mathrm{a}} \leqslant -\lambda_{\min}(\boldsymbol{\Lambda}_2)(z_1^2 + z_2^2 + z_3^2) \triangleq -W_2, \tag{33}$$

where $\lambda_{\min}(\boldsymbol{\Lambda}_2)$ is the minimal eigenvalue of matrix $\boldsymbol{\Lambda}_2$. Then considering the result in the feedback linearization control, it can be concluded that asymptotic tracking performance can also be achieved with the developed adaptive controller, i.e., $z_1 \to 0$ as $t \to \infty$.

The verification of this traditional adaptive control method can be found in many of the author's publications listed in the references.

3.3 Nonlinear robust control

In Case 3, the hydraulic system only exists uncertain nonlinearities and parametric uncertainties are neglected. Utilize the true values or nominal values of the physical parameters in the subsequent nonlinear robust controller design. Define the nominal value set $\boldsymbol{\theta}_{\mathrm{n}} = [\theta_{1\mathrm{n}}, \theta_{2\mathrm{n}}, \theta_{3\mathrm{n}}, \theta_{4\mathrm{n}}, \theta_{5\mathrm{n}}, \theta_{6\mathrm{n}}]^{\mathrm{T}}$. The system model for this case can be given by

$$\begin{cases} \dot{x}_1 = x_2 \\ \dot{x}_2 = \theta_1 x_3 - \theta_2 x_2 - \theta_3 S_f(x_2) - \dfrac{f_e(t)}{m} \\ \dot{x}_3 = \theta_4 f_1 u - \theta_5 f_2 - \theta_6 f_3 + q(t) \end{cases}. \quad (34)$$

Assumption 4: The uncertain nonlinearities $f_e(t)$ and $q(t)$ satisfy

$$|f_e(t)| \leqslant \delta_1,\ |q(t)| \leqslant \delta_2, \quad (35)$$

where δ_1 and δ_2 are known positive constants.

3.3.1 Nonlinear robust controller design

The error variables can be defined as in Eq. (16), and note the system model Eq. (34), describe the error dynamics as

$$\begin{cases} \dot{z}_2 = \theta_1(z_3 + \alpha_2) - \theta_2 x_2 - \theta_3 S_f(x_2) - \dfrac{f_e(t)}{m} - \dot{\alpha}_1 \\ \dot{z}_3 = \theta_4 f_1 u - \theta_5 f_2 - \theta_6 f_3 + q(t) - \dot{\alpha}_2 \end{cases}. \quad (36)$$

With the backstepping method, design the nonlinear robust controller u and α_2 as

$$\begin{cases} u = \dfrac{1}{\theta_{4n} f_1}[\theta_{5n} f_2 + \theta_{6n} f_3 + \dot{\alpha}_2 - k_3 z_3] \\ \alpha_2 = \dfrac{1}{\theta_n}[\theta_{2n} x_2 + \theta_{3n} S_f(x_2) + \dot{\alpha}_1 - k_2 z_2] \end{cases}. \quad (37)$$

Substituting the virtual control α_2 and the actual control input u into the error dynamics Eq. (36), it is

$$\begin{cases} \dot{z}_2 = \theta_1 z_3 - k_2 z_2 - \tilde{\boldsymbol{\theta}}_n^T \boldsymbol{\varphi}_2 - \dfrac{f_e(t)}{m} \\ \dot{z}_3 = -k_3 z_3 - \tilde{\boldsymbol{\theta}}_n^T \boldsymbol{\varphi}_3 + q(t) \end{cases}, \quad (38)$$

where $\tilde{\boldsymbol{\theta}}_n = \boldsymbol{\theta}_n - \boldsymbol{\theta}$ is the deviation between the true values and the nominal values of the system parameters.

3.3.2 Stability analysis

Theorem 3: By selecting the large control gains k_1, k_2, and k_3, the matrix $\boldsymbol{\Lambda}_3$ defined below will be positive definite,

$$\boldsymbol{\Lambda}_3 = \begin{bmatrix} k_1 & -\dfrac{1}{2} & 0 \\ -\dfrac{1}{2} & k_2 - \dfrac{1}{2} & -\dfrac{\theta_1}{2} \\ 0 & -\dfrac{\theta_1}{2} & k_3 - \dfrac{1}{2} \end{bmatrix}, \quad (39)$$

then the designed nonlinear robust controller Eq. (37) can achieve uniformly ultimately bounded tracking performance. In addition, the positive function

$$V_b = \frac{1}{2} z_1^2 + \frac{1}{2} z_2^2 + \frac{1}{2} z_3^2, \quad (40)$$

is bounded by

$$V_b(t) \leqslant V_b(0)\exp(-\lambda_1 t) + \frac{C_1}{\lambda_1}[1 - \exp(-\lambda_1 t)], \quad (41)$$

where $\lambda_1 = 2\lambda_{\min}(\boldsymbol{\Lambda}_3)$, in which $\lambda_{\min}(\boldsymbol{\Lambda}_3)$ is the minimal eigenvalue of matrix $\boldsymbol{\Lambda}_3$, and $C_1 = h_1^2/2 + h_2^2/2$ in which h_1 and h_2 are positive functions introduced in the proof.

Proof: Noting the error dynamics in Eq. (38), deduce the time derivative of $V_b(t)$ as follows:

$$\dot{V}_b = -k_1 z_1^2 - k_2 z_2^2 - k_3 z_3^2 + z_1 z_2 + \theta_1 z_2 z_3 + z_2\left[-\tilde{\boldsymbol{\theta}}_n^T \boldsymbol{\varphi}_2 - \frac{f_e(t)}{m}\right] + z_3\left[-\tilde{\boldsymbol{\theta}}_n^T \boldsymbol{\varphi}_3 + q(t)\right]. \quad (42)$$

Based on Assumptions 3 and 4, there exist positive functions $h_1(x, t)$ and $h_2(x, t)$ satisfying

$$\left|-\tilde{\boldsymbol{\theta}}_n^T \boldsymbol{\varphi}_2 - \frac{f_e(t)}{m}\right| \leqslant h_1(x,t),\ |-\tilde{\boldsymbol{\theta}}_n^T \boldsymbol{\varphi}_3 + q(t)| \leqslant h_2(x,t). \quad (43)$$

For example, let $h_1(x, t) = \|\boldsymbol{\varphi}_2\| \cdot \|\boldsymbol{\theta}_{\max} - \boldsymbol{\theta}_{\min}\| + \delta_1/m$, $h_2(x, t) = \|\boldsymbol{\varphi}_3\| \cdot \|\boldsymbol{\theta}_{\max} - \boldsymbol{\theta}_{\min}\| + \delta_2$. Then the right side of Eq. (42) can be upper bounded as

$$\begin{aligned} \dot{V}_b &\leqslant -k_1 z_1^2 - k_2 z_2^2 - k_3 z_3^2 + z_1 z_2 + \theta_1 z_2 z_3 + |z_2| h_1(x,t) + |z_3| h_2(x,t) \\ &\leqslant -k_1 z_1^2 - \left(k_2 - \frac{1}{2}\right) z_2^2 - \left(k_3 - \frac{1}{2}\right) z_3^2 + z_1 z_2 + \theta_1 z_2 z_3 + \frac{h_1^2(x,t)}{2} + \frac{h_2^2(x,t)}{2} \\ &\leqslant -\boldsymbol{Z}^T \boldsymbol{\Lambda}_3 \boldsymbol{Z} + \frac{h_1^2(x,t)}{2} + \frac{h_2^2(x,t)}{2} \leqslant -\lambda_1 V + C_1, \end{aligned} \quad (44)$$

which leads to Eq. (41) by employing the Comparing lemma [3]. The result in Eq. (41) indicates that uniformly ultimately bounded tracking performance can be obtained by the designed nonlinear robust controller. That is to say, the tracking error can be driven into a residual bounded set with the size of the order of the uncertain nonlinearity magnitude.

3.4 Nonlinear adaptive robust control

To handle uncertain nonlinearities and parametric uncertainties simultaneously in one controller, the nonlinear adaptive robust control method was synthesized in Ref. [2]. The system model for Case 4 is the same as in Eq. (34). To facilitate the nonlinear adaptive robust

controller design, besides Assumptions 1, 2, 3 and 4, the following discontinuous projection mapping is utilized.

Define the discontinuous projection as [2]:

$$\mathrm{Proj}_{\hat{\theta}_i}(\tau_i)=\begin{cases}0 & \text{if } \hat{\theta}_i=\theta_{i\max} \text{ and } \tau_i>0\\ 0 & \text{if } \hat{\theta}_i=\theta_{i\min} \text{ and } \tau_i<0\\ \tau_i & \text{otherwise}\end{cases}, \quad (45)$$

where $i=1, 2, \ldots, 6$, and is an adaptation function to be designed later.

With the adaptation law given by

$$\dot{\hat{\boldsymbol{\theta}}}=\mathrm{Proj}_{\hat{\boldsymbol{\theta}}}(\boldsymbol{\Gamma}\boldsymbol{\tau}) \text{ with } \boldsymbol{\theta}_{\min}\leqslant\hat{\boldsymbol{\theta}}(0)\leqslant\boldsymbol{\theta}_{\max}, \quad (46)$$

where $\boldsymbol{\Gamma}$ is a diagonal adaptation rate matrix, and $\boldsymbol{\Gamma}>0$. Therefore, the projection mapping proposed above with any adaptation function can guarantee [2]

$$(\mathbf{P1}) \qquad \hat{\boldsymbol{\theta}}\in\Omega_{\hat{\boldsymbol{\theta}}}\triangleq\{\hat{\boldsymbol{\theta}}:\boldsymbol{\theta}_{\min}\leqslant\hat{\boldsymbol{\theta}}\leqslant\boldsymbol{\theta}_{\max}\}, \quad (47)$$

$$(\mathbf{P2}) \qquad \tilde{\boldsymbol{\theta}}^{\mathrm{T}}[\boldsymbol{\Gamma}^{-1}\mathrm{Proj}_{\hat{\boldsymbol{\theta}}}(\boldsymbol{\Gamma}\boldsymbol{\tau})-\boldsymbol{\tau}]\leqslant 0, \quad \forall\boldsymbol{\tau}. \quad (48)$$

3.4.1 Nonlinear adaptive robust controller design

The error variables can be defined as in Eq. (16), and note the system model Eq. (34), described the error dynamics as in Eq. (36). Then based on the backstepping design procedure, the virtual control law α_2 and the nonlinear adaptive robust controller u and can be synthesized as

$$\begin{aligned}\alpha_2&=\frac{1}{\hat{\theta}_1}(\alpha_{2\mathrm{a}}+\alpha_{2\mathrm{s}}),\\ \alpha_{2\mathrm{a}}&=\hat{\theta}_2x_2+\hat{\theta}_3S_{\mathrm{f}}(x_2)+\dot{\alpha}_1,\\ \alpha_{2\mathrm{s}}&=\alpha_{2\mathrm{s}1}+\alpha_{2\mathrm{s}2},\\ \alpha_{2\mathrm{s}1}&=-k_2z_2,\\ \alpha_{2\mathrm{s}2}&=-k_{\mathrm{s}2}z_2\triangleq-\frac{\psi_2}{2\varepsilon_2}z_2,\end{aligned} \quad (49)$$

$$\begin{aligned}u&=\frac{1}{\hat{\theta}_4f_1}(u_{\mathrm{a}}+u_{\mathrm{s}}),\\ u_{\mathrm{a}}&=\hat{\theta}_5f_2+\hat{\theta}_6f_3+\dot{\alpha}_2,\\ u_{\mathrm{s}}&=u_{\mathrm{s}1}+u_{\mathrm{s}2},\\ u_{\mathrm{s}1}&=-k_3z_3,\\ u_{\mathrm{s}2}&=-k_{\mathrm{s}3}z_3\triangleq-\frac{\psi_3}{2\varepsilon_3}z_3,\end{aligned} \quad (50)$$

where ε_2, ε_3 are positive constants, $k_{\mathrm{s}2}$ and $k_{\mathrm{s}3}$ are positive nonlinear gains, and ψ_2 and ψ_3 are smooth functions satisfying

$$\begin{cases}\psi_2\geqslant\|\boldsymbol{\theta}_{\mathrm{M}}\|^2\|\boldsymbol{\varphi}_2\|^2+\delta_1^2/m^2\\ \psi_3\geqslant\|\boldsymbol{\theta}_{\mathrm{M}}\|^2\|\boldsymbol{\varphi}_3\|^2+\delta_2^2\end{cases}, \quad (51)$$

in which $\boldsymbol{\theta}_{\mathrm{M}}=\boldsymbol{\theta}_{\max}-\boldsymbol{\theta}_{\min}$.

Substituting the virtual control α_2 and the actual control input u into the error dynamics Eq. (36), it is

$$\begin{cases}\dot{z}_2=\theta_1z_3-k_2z_2+\alpha_{2s2}-\tilde{\boldsymbol{\theta}}^{\mathrm{T}}\boldsymbol{\varphi}_2-f_{\mathrm{e}}(t)/m\\ \dot{z}_3=-k_3z_3+u_{s2}-\tilde{\boldsymbol{\theta}}^{\mathrm{T}}\boldsymbol{\varphi}_3+q(t)\end{cases}. \quad (52)$$

3.4.2 Stability analysis

Theorem 4: Based on the projection type adaptive law in Eq. (46) and adaptation function $\boldsymbol{\tau}=\boldsymbol{\varphi}_2z_2+\boldsymbol{\varphi}_2z_3$, by selecting large control gains k_1, k_2, and k_3, the matrix $\boldsymbol{\Lambda}_2$ described in Eq. (30) will be positive definite, and the designed nonlinear adaptive robust controller Eq. (50) can guarantee:

A. Generally, all signals are bounded and uniformly ultimately bounded tracking performance can be achieved.

B. Provided after a finite time, the system is only subjected to the parametric uncertainties (i.e., $f_{\mathrm{e}}(t)=0$, $q(t)=0$ after a finite time), asymptotic tracking performance can be also obtained, i.e., $z_1\to 0$ as $t\to\infty$.

Proof: For the general case, choosing the positive Lyapunov function $V_{\mathrm{b}}(t)$ defined in Eq. (40) and its time derivative can be written as:

$$\begin{aligned}\dot{V}_{\mathrm{b}}=&-k_1z_1^2-k_2z_2^2-k_3z_3^2+z_1z_2+\theta_1z_2z_3\\ &+z_2\left[\alpha_{2s2}-\tilde{\boldsymbol{\theta}}^{\mathrm{T}}\boldsymbol{\varphi}_2-\frac{f_{\mathrm{e}}(t)}{m}\right]\\ &+z_3\left[u_{s2}-\tilde{\boldsymbol{\theta}}_{\mathrm{n}}^{\mathrm{T}}\boldsymbol{\varphi}_3+q(t)\right].\end{aligned} \quad (53)$$

Since the following inequality holds:

$$\begin{aligned}z_2\left[\alpha_{2s2}-\tilde{\boldsymbol{\theta}}^{T}\boldsymbol{\varphi}_2-\frac{f_{\mathrm{e}}(t)}{m}\right]&=-\frac{\psi_2}{2\varepsilon_2}z_2^2-\tilde{\boldsymbol{\theta}}^{\mathrm{T}}\boldsymbol{\varphi}_2z_2-\frac{f_{\mathrm{e}}(t)}{m}z_2\\ &\leqslant-\frac{\psi_2}{2\varepsilon_2}z_2^2+\|\tilde{\boldsymbol{\theta}}^{\mathrm{T}}\boldsymbol{\varphi}_2\||z_2|+\frac{\delta_1}{m}|z_2|.\\ &\leqslant-\frac{\|\boldsymbol{\theta}_{\mathrm{M}}\|^2\|\boldsymbol{\varphi}_2\|^2}{2\varepsilon_2}z_2^2+\|\tilde{\boldsymbol{\theta}}^{\mathrm{T}}\boldsymbol{\varphi}_2\||z_2|\\ &\quad-\frac{\delta_1^2/m^2}{2\varepsilon_2}z_2^2+\frac{\delta_1}{m}|z_2|\leqslant\varepsilon_2.\end{aligned} \quad (54)$$

Similarly,

$$z_3\left[u_{s2}-\tilde{\boldsymbol{\theta}}_{\mathrm{n}}^{\mathrm{T}}\boldsymbol{\varphi}_3+q(t)\right]\leqslant\varepsilon_3. \quad (55)$$

Thus, combing Eqs. (54) and (55), the right side of Eq. (53) can be upper bounded as

$$\dot{V}_b \leqslant -k_1 z_1^2 - k_2 z_2^2 - k_3 z_3^2 + z_1 z_2 + \theta_1 z_2 z_3 + \varepsilon_2 + \varepsilon_3$$

$$\leqslant -\boldsymbol{Z}^T \boldsymbol{\Lambda}_2 \boldsymbol{Z} + C_2 \leqslant -\lambda_2 V_b + C_2, \quad (56)$$

where $C_2 = \varepsilon_2 + \varepsilon_3$, and $\lambda_2 = 2\lambda_{\min}(\boldsymbol{\Lambda}_2)$.

By employing the Comparing lemma [3], it can be concluded from Eq. (56) that the positive function $V_b(t)$ is bounded by

$$V_b(t) \leqslant V_b(0)\exp(-\lambda_2 t) + \frac{C_2}{\lambda_2}[1 - \exp(-\lambda_2 t)], \quad (57)$$

which leads to Part A of Theorem 4.

Then, consider the proof of Part B of Theorem 4, choosing the positive function $V_a(t)$ defined in Eq. (31) and its time derivative can be written as

$$\dot{V}_a = -k_1 z_1^2 - k_2 z_2^2 - k_3 z_3^2 + z_1 z_2 + \theta_1 z_2 z_3$$

$$+ z_2\left(\alpha_{2s2} - \tilde{\boldsymbol{\theta}}^T \boldsymbol{\varphi}_2\right) + z_3\left(u_{s2} - \tilde{\boldsymbol{\theta}}_n^T \boldsymbol{\varphi}_3\right)$$

$$+ \tilde{\boldsymbol{\theta}}^T \Gamma^{-1} \dot{\hat{\boldsymbol{\theta}}}. \quad (58)$$

Considering the property P2 in Eq. (48) and the definition of , thus

$$\dot{V}_a \leqslant -\boldsymbol{Z}^T \boldsymbol{\Lambda}_2 \boldsymbol{Z} \leqslant -\lambda_{\min}(\boldsymbol{\Lambda}_2)(z_1^2 + z_2^2 + z_3^2) \triangleq -W_2. \quad (59)$$

Similar to the proof of traditional adaptive controller, by applying Barbalat's lemma, the Part B of Theorem 4 can be derived.

3.4.3 Experimental verification

In order to verify the effectiveness of the developed adaptive robust control (ARC) controller, the experimental results were obtained in Ref. [18] on a hydraulic load simulator by comparing the ARC controller with industrial PID controller. Although the torque tracking control was considered in Ref. [18], the designed concept was the same as the above nonlinear ARC control design. Hence, the experimental results in Ref. [18] are utilized to illustrate the high-performance feature of nonlinear ARC control. The sinusoidal movement of the hydraulic actuator system is with 20° amplitude and 1 Hz frequency. The torque desired trajectory is the sinusoidal signal with 1000 N·m amplitude and 5 Hz frequency. Figures 3 and 4 demonstrate the torque tracking performances under PID controller and the proposed nonlinear ARC controller respectively. As a result, the maximum tracking error about 50 N·m is obtained by nonlinear ARC controller, while under the conventional PID controller, the maximum tracking error is huge. Hence, the developed ARC controller achieves better tracking performance than PID

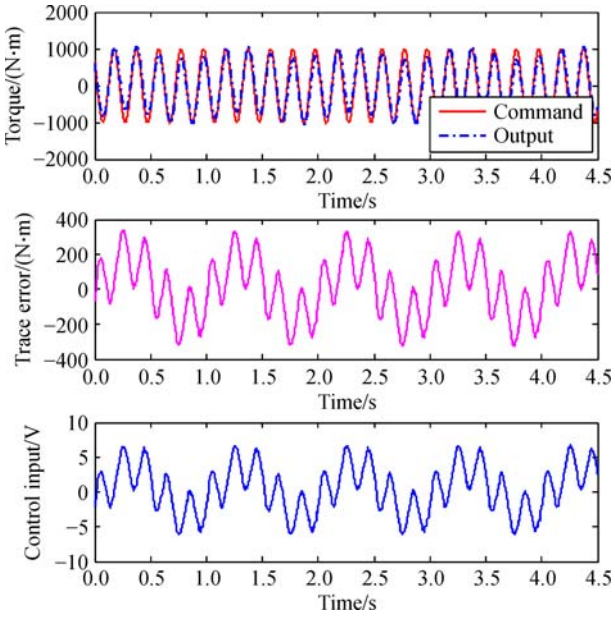

Fig. 3 Tracking performance under PID controller

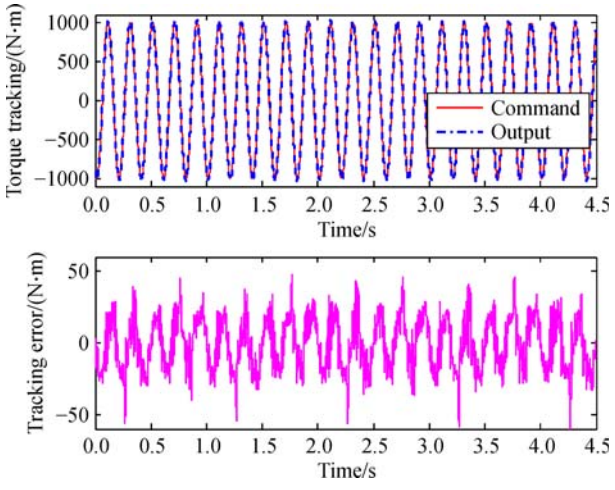

Fig. 4 Tracking performance under ARC controller

controller. Referring to Ref. [18], the readers can see more details about the experiments.

3.5 Nonlinear adaptive integral robust control

It can be found from Case 4 that although the developed nonlinear adaptive robust controller can simultaneously handle the parametric uncertainties and uncertain nonlinearities, only bounded tracking performance can be obtained for the general case, i.e., the system is subjected to both parametric uncertainties and uncertain nonlinearities. Hence, in Case 5, a nonlinear adaptive integral robust controller is present to obtain excellent asymptotic tracking performance with both parametric uncertainties and uncertain nonlinearities.

As mentioned in Remark 1, the internal leakage $q_L(P_L)$ is typically modeled by a linear term with respect to the load pressure P_L, i.e., $q_L(P_L)= C_tP_L$, however, this model might be not precise for different actuators. Hence, in Ref. [7], to improve the tracking performance, an internal leakage identification experiment was conducted for a valve-controlled bidirectional hydraulic motor to obtain a more accurate internal leakage model which is given below

$$q_L = c_1P_L^2 + c_2P_L + c_3, \tag{60}$$

where c_1, c_2, and c_3 are leakage coefficients.

Based on the physical model Eqs. (1), (4), (5), and (60), it can be redefined the state variables as $\boldsymbol{x} =[x_1, x_2, x_3]^T=[y, \dot{y}, AP_L/m]^T$, and the unknown parameter set $\boldsymbol{\theta} = [\theta_1, \theta_2, \theta_3, \theta_4, \theta_5]^T$, where $\theta_1 = \beta_e k_t$, $\theta_2 = \beta_e$, $\theta_3 = \beta_e c_1$, $\theta_4 = \beta_e c_2$, and $\theta_5 = \beta_e c_3$. In addition, the modeled friction $f_r(t)$ in Eq. (2) is considered to verify the robustness of the designed nonlinear integral robust term in this case. Then describe the specific system model below:

$$\begin{cases} \dot{x}_1 = x_2 \\ \dot{x}_2 = x_3 - bx_2 + d(t) \\ \dot{x}_3 = \theta_1 g_1 u - \theta_2 g_2 - \theta_3 g_3 - \theta_4 g_4 - \theta_5 g_5 \end{cases}, \tag{61}$$

where $b = B/m$, $d(t)= f_e(t)/m$, and

$$g_1 = \frac{A}{m}\left(\frac{R_1}{V_1} + \frac{R_2}{V_2}\right),$$

$$g_2 = \frac{A^2}{m}\left(\frac{1}{V_1} + \frac{1}{V_2}\right)x_2,$$

$$g_3 = \frac{m}{A}\left(\frac{1}{V_1} + \frac{1}{V_2}\right)x_3^2,$$

$$g_4 = \left(\frac{1}{V_1} + \frac{1}{V_2}\right)x_3,$$

$$g_5 = \frac{A}{m}\left(\frac{1}{V_1} + \frac{1}{V_2}\right).$$

With the similar method to design the nonlinear controller in Case 4, the discontinuous projection mapping and parameter adaptation proposed in Eqs. (45) and (46) are also utilized. In addition, make an assumption as follows.

Assumption 5: The uncertain nonlinearities $d(t)$ is smooth enough such that

$$|\dot{d}| \leqslant \sigma_1,\ |\ddot{d}| \leqslant \sigma_2, \tag{62}$$

where σ_1 and σ_2 are known positive constants.

For the rationality of the Assumption 5, one may argue that the assumption is too strict since the friction is typically discontinuous. It can be explained that although frictions are modeled as discontinuous functions generally, there are still some continuous friction models for model-based controller design, because none of physical actuators can produce discontinuous force to compensate the discontinuous friction effects, an example of continuous friction models will be given in the next section of this paper.

3.5.1 Nonlinear adaptive integral robust controller design

Besides the error variables defined in Eq. (16), an auxiliary error signal r is defined as follows to facilitate the nonlinear adaptive integral robust controller design

$$r = \dot{z}_2 + k_2z_2. \tag{63}$$

Based on the backstepping design procedure, design the virtual control law α_2 and the nonlinear adaptive integral robust controller u as

$$\alpha_2 = \alpha_{2a} + \alpha_{2s},$$

$$\alpha_{2a} = \dot{\alpha}_1 - k_2z_2 + bx_2,$$

$$\alpha_{2s} = \alpha_{2s1} + \alpha_{2s2},$$

$$\alpha_{2s1} = -k_rz_2,$$

$$\alpha_{2s2} = -\int_0^t [k_rk_2z_2 + \beta \mathrm{sign}(z_2)]\mathrm{d}\nu, \tag{64}$$

$$\begin{cases} u = u_a + u_s \\ u_a = \dfrac{1}{\hat{\theta}_1 g_1}(\hat{\theta}_2 g_2 + \hat{\theta}_3 g_3 + \hat{\theta}_4 g_4 + \hat{\theta}_5 g_5 + \dot{\alpha}_2), \\ u_s = -\dfrac{k_3 z_3}{g_1} \end{cases} \tag{65}$$

where $k_r > 0$ is a feedback gain, and β is a positive feedback gain.

Substituting the virtual control law α_2 and the actual control input u into the dynamics of r and z_3, it can be obtained

$$\dot{r} = -\boldsymbol{\varphi}^T\tilde{\boldsymbol{\theta}} - k_3\theta_1 z_3 - k_r r - \beta \mathrm{sign}(z_2) + \dot{d}, \tag{66}$$

$$\dot{z}_3 = -\boldsymbol{\varphi}^T\tilde{\boldsymbol{\theta}} - k_3\theta_1 z_3, \tag{67}$$

where $\boldsymbol{\varphi} = [f_1u_a, -f_2, -f_3, -f_4, -f_5]^T$ is the regressor for parameter adaptation.

3.5.2 Stability analysis

Lemma 1: Define an auxiliary function $L(t)$ as

$$L(t) = r\left[\dot{d} - \beta \mathrm{sign}(z_2)\right], \tag{68}$$

where β is the gain and satisfies the following sufficient condition:

$$\beta \geqslant \sigma_1 + \frac{1}{k_2}\sigma_2, \tag{69}$$

thus, the function $P(t)$ defined below is always positive,

$$P(t) = \beta|z_2(0)| - z_2(0)\dot{d}(0) - \int_0^t L(\nu)\mathrm{d}\nu. \tag{70}$$

The detailed proof of Lemma 1 can be found in Ref. [7].

Theorem 5: Based on the projection type adaptive law in Eq. (46) and adaptation function $\boldsymbol{\tau} = \boldsymbol{\varphi}(r + z_3)$, if the gain β satisfies Eq. (69) and the feedback gains k_1, k_2, k_3 and k_r are large enough, the matrix $\boldsymbol{\Lambda}_4$ developed below is positive definite

$$\boldsymbol{\Lambda}_4 = \begin{bmatrix} k_1 & -\frac{1}{2} & 0 & 0 \\ -\frac{1}{2} & k_2 & -\frac{1}{2} & 0 \\ 0 & -\frac{1}{2} & k_r & \frac{1}{2}\theta_1 k_3 \\ 0 & 0 & \frac{1}{2}\theta_1 k_3 & \theta_1 k_3 \end{bmatrix}, \tag{71}$$

then the designed nonlinear adaptive integral robust controller Eq. (65) guarantees that all system signals are bounded, in addition, asymptotic output tracking performance can be obtained, i.e., $z_1 \to 0$ as $t \to \infty$.

Proof: Define a positive Lyapunov function $V_2(t)$ as follows:

$$V_2 = \frac{1}{2}z_1^2 + \frac{1}{2}z_2^2 + \frac{1}{2}z_3^2 + \frac{1}{2}r^2 + \frac{1}{2}\tilde{\boldsymbol{\theta}}^{\mathrm{T}}\boldsymbol{\Gamma}^{-1}\tilde{\boldsymbol{\theta}} + P(t). \tag{72}$$

Note the error dynamics in Eqs. (16), (63), (66), and (67), and the definition of $P(t)$ in Eq. (70), the time derivative of $V_2(t)$ can be expressed by

$$\begin{aligned} \dot{V}_2 &= z_1\dot{z}_1 + z_2\dot{z}_2 + z_3\dot{z}_3 + r\dot{r} + \tilde{\boldsymbol{\theta}}^{\mathrm{T}}\boldsymbol{\Gamma}^{-1}\dot{\hat{\boldsymbol{\theta}}} + \dot{P} \\ &= -k_1 z_1^2 + z_1 z_2 - k_2 z_2^2 + z_2 r - k_r r^2 - k_3\theta_1 z_3 r \\ &\quad -k_3\theta_1 z_3^2 + \tilde{\boldsymbol{\theta}}^{\mathrm{T}}\boldsymbol{\Gamma}^{-1}\left(\dot{\hat{\boldsymbol{\theta}}} - \boldsymbol{\Gamma}\boldsymbol{\tau}\right). \end{aligned} \tag{73}$$

Utilizing the property P2 in Eq. (48), it can be obtained

$$\dot{V}_2 \leqslant -z^{\mathrm{T}}\boldsymbol{\Lambda}_4 z \leqslant -\lambda_{\min}(\boldsymbol{\Lambda}_4)(z_1^2 + z_2^2 + z_3^2 + r^2) \triangleq -W_3, \tag{74}$$

where $\lambda_{\min}(\boldsymbol{\Lambda}_4)$ is the minimal eigenvalue of matrix $\boldsymbol{\Lambda}_4$. According to Barbalat's lemma, $W_3 \to 0$ as $t \to \infty$, the results in Theorem 5 can be obtained.

Remark 3: Noting that the nonlinear adaptive integral robust control presented above can achieve asymptotic tracking performance only under matched uncertain nonlinearity and the parametric uncertainty in the second channel cannot handle by adaptive method. In addition, the integral robust feedback gain β above nonlinear adaptive integral robust controller needs to be selected by the designer, which leads to some design conservatism and difficulty of gain tuning in practical application. Based on the acceleration based state-space model in Eq. (13), all the uncertain nonlinearities and parametric uncertainties are considered, and asymptotic tracking performance can be obtained in Refs. [8,19]. The adaptation of the integral robust feedback gain β was also realized in Refs. [20,21].

3.5.3 Experimental verification

In order to demonstrate the superiority of the developed nonlinear adaptive integral robust controller, the experimental results were present in Ref. [7] for a valve-controlled bidirectional hydraulic motor. The nonlinear adaptive integral robust controller or nonlinear adaptive RISE-based controller (ARISE) was compared with nonlinear ARC controller and PID controller. The experiment was divided into three parts based on the employed desired motion trajectory. The three controllers were run to track a normal-level sinusoidal-like trajectory, x_{1d}= 10sin(3.14t) ·(1–exp(–0.01t^3))°. The tracking performance of ARISE, ARC, and PID are demonstrated in Figs. 5 and 6. The parameter adaptation process of ARISE is presented in Fig. 7. To further test the robustness of the developed ARISE against unmodeled uncertainties, a slow motion command x_{1d} = 0.1sin(0.628t)(1–exp(–0.01t^3))° is given. For the slow-motion case, Figs. 8 and 9 demonstrate the tracking performance of the three controllers. At last, The three controllers are then required to track a fast motion command given by x_{1d} = 10sin(12.56t)(1–exp(–0.01t^3))°. Figures 10 and 11 show the corresponding tracking performance. All the experimental results explain that the developed ARISE controller obtains the best transient and steady-state tracking performance. Referring to Ref. [7],

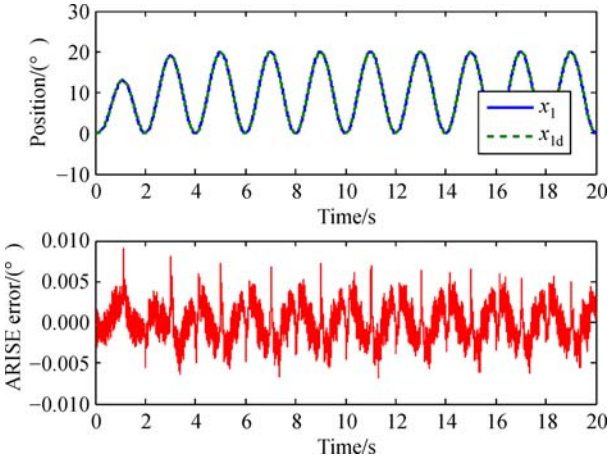

Fig. 5 Tracking performance of ARISE for normal motion

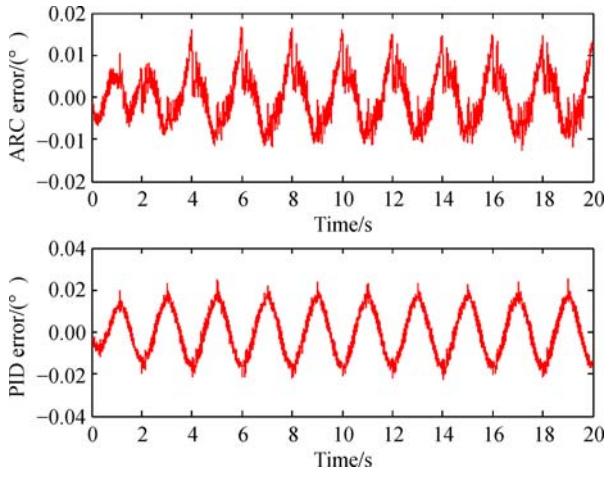

Fig. 6 Tracking errors of ARC and PID for normal motion

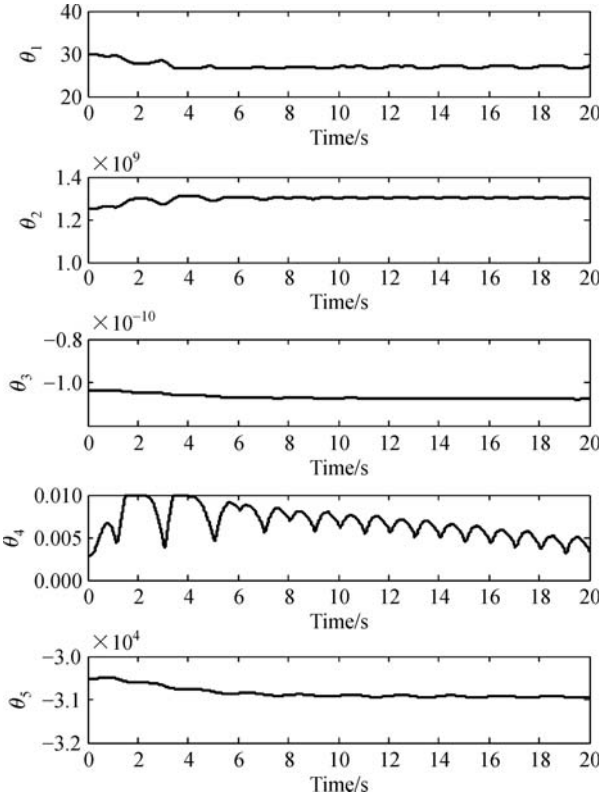

Fig. 7 Parameter estimation of ARISE for normal motion

the reader can see more details about the experimental results.

3.6 Nonlinear adaptive repetitive control

In Case 6, the hydraulic system performing repetitive tasks is considered. The nominal values of the system parameters are assumed to be known, which can simplify the controller design. That is, all system parameters

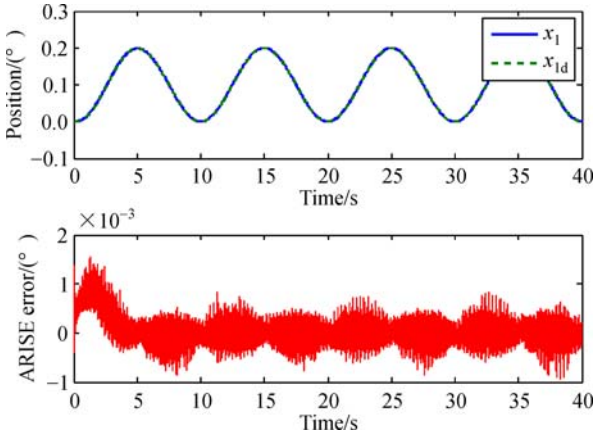

Fig. 8 Tracking performance of ARISE for slow motion

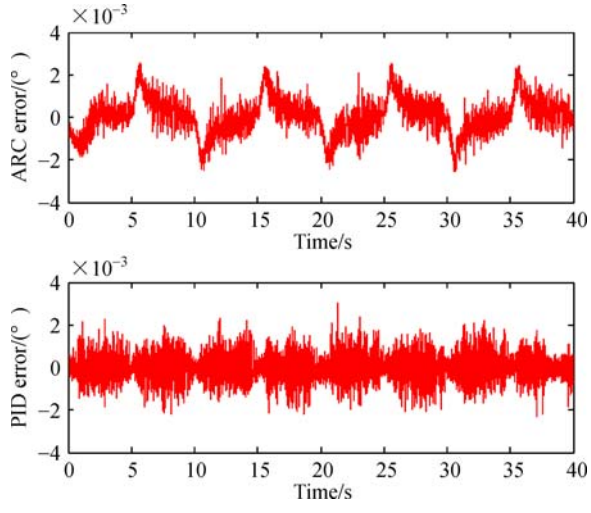

Fig. 9 Tracking errors of ARC and PID controllers for slow motion

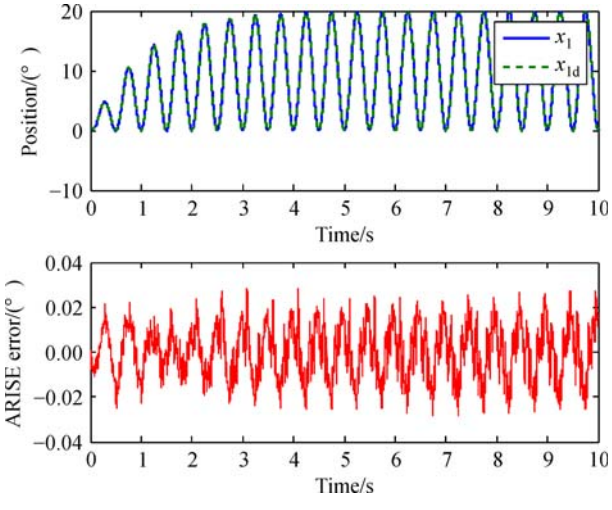

Fig. 10 Tracking performance of ARISE for fast motion

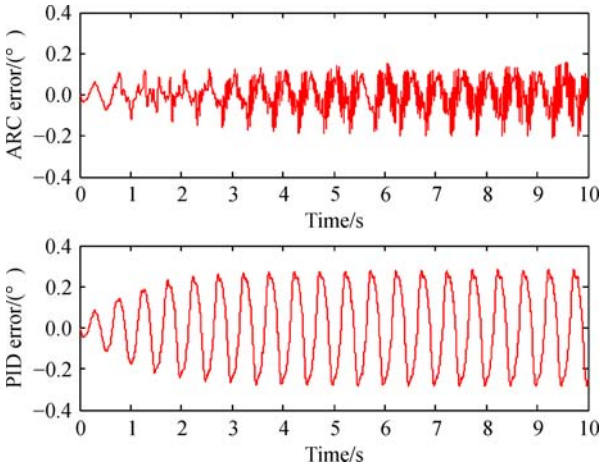

Fig. 11 Tracking errors of ARC and PID controllers for fast motion

(including J, A, B, A_f, V_{01}, V_{02}, β_e, k_t, and C_t) can be used when designing the controller. However, because of the changes in component wear and temperature, the system is generally subjected to parametric uncertainties. Hence the specific system model for this case can be given as

$$\begin{cases} \dot{x}_1 = x_2 \\ m\dot{x}_2 = Ax_3 - Bx_2 - A_f S_f(x_2) - d_1(x_1, x_2), \\ \dot{x}_3 = F_1 u - F_2 - d_2(x_1, x_2) \end{cases} \tag{75}$$

where

$$F_1 = \left(\frac{R_1}{V_1} + \frac{R_2}{V_2}\right)\beta_e k_t,$$

$$F_2 = \beta_e\left(\frac{1}{V_1} + \frac{1}{V_2}\right)(Ax_2 + C_t x_3).$$

In Eq. (75), two additional terms $d_1(x_1, x_2)$ and $d_2(x_1, x_2)$ are assumed to be continuous differentiable functions, representing all modelling uncertainties. Therefore, when designing the nonlinear adaptive repetitive controller, the problem of unknown nonlinearities $d_1(x_1, x_2)$ and $d_2(x_1, x_2)$ is the primary focus to be dealt with. The case with non-periodic disturbanes will be discussed later.

In Eq. (75), although $d_1(x_1, x_2)$ and $d_2(x_1, x_2)$ are unknown, because of the periodicity of the tracked trajectory x_{1d}, a certain periodicity will be observed after some cycles. Therefore, repetitive control may be an excellent tool to eliminate the periodic-like disturbances $d_1(x_1, x_2)$ and $d_2(x_1, x_2)$. On the basis of this important analysis, Eq. (75) can be rewritten as

$$\begin{cases} \dot{x}_1 = x_2 \\ m\dot{x}_2 = Ax_3 - Bx_2 - A_f S_f(x_2) - d_1(x_{1d}, \dot{x}_{1d}) - \Delta_1, \\ \dot{x}_3 = F_1 u - F_2 - d_2(x_{1d}, \dot{x}_{1d}) - \Delta_2 \end{cases} \tag{76}$$

where Δ_1 and Δ_2 represent approximation errors defined by

$$\Delta_1 \triangleq d_1(x_1, x_2) - d_1(x_{1d}, \dot{x}_{1d}),$$

$$\Delta_2 \triangleq d_2(x_1, x_2) - d_2(x_{1d}, \dot{x}_{1d}). \tag{77}$$

$D_{1d}(t)$ and $D_{2d}(t)$ are utilized to represent $d_1(x_{1d}, \dot{x}_{1d})$ and $d_2(x_{1d}, \dot{x}_{1d})$ to simplify the controller design. For the repetitive tasks, since the desired signal x_{1d} is periodic, i.e.,

$$x_{1d}(t - T) = x_{1d}(t), \tag{78}$$

where T is the known period, $D_{1d}(t)$ and $D_{2d}(t)$ are only related to x_{1d} and $\dot{x}_{1d}$, the unknown nonlinear functions D_{1d}(t) and $D_{2d}(t)$ are also periodic, i.e.,

$$D_{1d}(t - T) = D_{1d}(t),$$

$$D_{2d}(t - T) = D_{2d}(t). \tag{79}$$

By utilizing Fourier series, represent the periodic nonlinear functions $D_{1d}(t)$ and $D_{2d}(t)$ as follows:

$$\begin{cases} D_{1d}(t) = \dfrac{A_0}{2} + \displaystyle\sum_{n=1}^{\infty}(A_n \cos n\omega t + B_n \sin n\omega t) \\ D_{2d}(t) = \dfrac{C_0}{2} + \displaystyle\sum_{n=1}^{\infty}(C_n \cos n\omega t + D_n \sin n\omega t) \end{cases}, \tag{80}$$

where $\omega = 2\pi/T$. Denote $D_{1d}(t)$ and $D_{2d}(t)$ by finite frequency components because the mechanical system is physically equivalent to a low-pass filter, i.e., a Fourier series can be used to approximate them with finite terms in implementation [22]:

$$\begin{cases} D_{1d}(t) = \dfrac{A_0}{2} + \displaystyle\sum_{n=1}^{m}(A_n \cos n\omega t + B_n \sin n\omega t), \quad m < \infty \\ D_{2d}(t) = \dfrac{C_0}{2} + \displaystyle\sum_{n=1}^{m}(C_n \cos n\omega t + D_n \sin n\omega t), \quad m < \infty \end{cases}. \tag{81}$$

The unknown but constant parameter set $\boldsymbol{\theta}$ can be defined as $\boldsymbol{\theta} = [A_0/2, A_1, B_1, \ldots, A_m, B_m, C_0/2, C_1, D_1, \ldots, C_m, D_m]^T$ to simplify the system design. Thus, with Eq. (81), the system model Eq. (76) can be rewritten to

$$\begin{cases} \dot{x}_1 = x_2 \\ m\dot{x}_2 = Ax_3 - Bx_2 - A_f S_f(x_2) - \Phi_1^T \boldsymbol{\theta} - \Delta_1, \\ \dot{x}_3 = f_1 u - f_2 - \Phi_2^T \boldsymbol{\theta} - \Delta_2 \end{cases} \tag{82}$$

where

$$\begin{cases} \Phi_1 = [1, \cos\omega t, \sin\omega t, \ldots, \cos m\omega t, \sin m\omega t, 0, \ldots, 0]^T \\ \Phi_2 = [0, \ldots, 0, 1, \cos\omega t, \sin\omega t, \ldots, \cos m\omega t, \sin m\omega t]^T \end{cases}. \tag{83}$$

For the case with non-periodic disturbances, transform the system model Eq. (75) to

$$\begin{cases} \dot{x}_1 = x_2 \\ m\dot{x}_2 = Ax_3 - Bx_2 - A_f S_f(x_2) - d_1(x_1,x_2) - \eta_1(t) \\ \dot{x}_3 = F_1 u - F_2 - d_2(x_1,x_2) - \eta_1(t) \end{cases} . \quad (84)$$

In Eq. (84), the unknown nonlinear functions $d_1(x_1, x_2)$ and $d_2(x_1, x_2)$ will present some certain periodicities because they are state-dependent disturbances. In addition, the unknown non-periodic effects in actual systems are put in $\eta_1(t)$ and $\eta_2(t)$.

On the basis of the formulation method proposed in Part A, transfer the design model Eq. (16) to

$$\begin{cases} \dot{x}_1 = x_2 \\ m\dot{x}_2 = Ax_3 - Bx_2 - A_f S_f(x_2) - \boldsymbol{\Phi}_1^T \boldsymbol{\theta} - \tilde{\Delta}_1(t) \\ \dot{x}_3 = F_1 u - F_2 - \boldsymbol{\Phi}_2^T \boldsymbol{\theta} - \tilde{\Delta}_2(t) \end{cases} , \quad (85)$$

where $\tilde{\Delta}_1$ and $\tilde{\Delta}_2$ are lumped uncertain nonlinearities, which are defined by

$$\tilde{\Delta}_1(t) \triangleq \Delta_1 + \eta_1(t),\ \tilde{\Delta}_2(t) \triangleq \Delta_2 + \eta_2(t). \quad (86)$$

Assumption 6: The uncertain nonlinearities existed in Eq. (85) are usually bounded by

$$|\tilde{\Delta}_1(t)| \leqslant \delta_1(t),\ |\tilde{\Delta}_2(t)| \leqslant \delta_2(t), \quad (87)$$

where $\delta_1(t)$ and $\delta_2(t)$ are bounded unknown functions.

3.6.1 Nonlinear adaptive repetitive controller design

Define the error variables as in Eq. (16), and note the system model Eq. (82), the error dynamics can be written as

$$\begin{cases} m\dot{z}_2 = A(z_3 + \alpha_2) - m\dot{\alpha}_1 - Bx_2 - A_f S_f(x_2) - \Phi_1^T \boldsymbol{\theta} - \Delta_1 \\ \dot{z}_3 = F_1 u - F_2 - \Phi_2^T \boldsymbol{\theta} - \Delta_2 - \dot{\alpha}_2 \end{cases} . \quad (88)$$

Following the design process of the backstepping method, the virtual control law α_2 and the nonlinear adaptive repetitive control law u and can be given as

$$\alpha_2 = \frac{1}{A}\left[m\dot{\alpha}_1 + Bx_2 + A_f S_f(x_2) + \Phi_1^T \hat{\boldsymbol{\theta}} - \left(k_2 + \frac{1}{2}\right) z_2 \right], \quad (89)$$

$$u = \frac{1}{F_1}\left[F_2 + \Phi_2^T \hat{\boldsymbol{\theta}} + \dot{\alpha}_{2c} - \left(k_3 + \frac{1}{2}\right) z_3 \right], \quad (90)$$

where

$$\dot{\alpha}_{2c} = \frac{\partial \alpha_2}{\partial t} + \frac{\partial \alpha_2}{\partial x_1} x_2 + \frac{\partial \alpha_2}{\partial x_2} \frac{1}{J} \cdot \left[Ax_3 - Bx_2 - A_f S_f(x_2) - \Phi_1^T \hat{\boldsymbol{\theta}} \right] + \frac{\partial \alpha_2}{\partial \hat{\theta}} \dot{\hat{\boldsymbol{\theta}}} . \quad (91)$$

3.6.2 Stability analysis

Theorem 6.1: As the adaptation law mentioned in Eq. (46) and the adaptation function given below

$$\boldsymbol{\tau} = -\Phi_1 z_2 - \left(\Phi_2 - \frac{\partial \alpha_2}{\partial x_2} \frac{1}{J} \Phi_1 \right) z_3, \quad (92)$$

then in the closed-loop operation, the mentioned control law Eq. (90) can ensure that all system signals are in a bounded range, and can also get asymptotic tracking performance, i.e., $z_1 \to 0$ as $t \to \infty$; when the control gain k_1, k_2, and k_3 are defined sufficiently large, the matrix $\boldsymbol{\Lambda}_1$ defined in Eq. (20) can be guaranteed to be positive definite.

Theorem 6.2: By choosing appropriate feedback gains k_1, k_2 and k_3, then the matrix $\boldsymbol{\Lambda}_1$ can be guaranteed to be positive definite, then the raised control law Eq. (90) under Assumption 6 ensures that

A. Generally speaking, all the signals are guaranteed bounded. Furthermore, the Lyapunov function $V_1(t)$ described in Eq. (21) is bounded by

$$V_1(t) \leqslant \exp(-\kappa t) V_1(0) + \frac{||\delta(t)||_\infty^2}{\kappa} [1 - \exp(-\kappa t)], \quad (93)$$

where $\kappa = 2\min\{\lambda_{\min}(\boldsymbol{\Lambda}_1), \lambda_{\min}(\boldsymbol{\Lambda}_1)/m\}$ is the exponentially converging rate, $\delta(t)$ is an unknown but bounded function satisfying

$$\delta(t) \geqslant \max\left\{ \|\boldsymbol{\Phi}_1\| \cdot \|\boldsymbol{\theta}_M\| + \delta_1(t), \|\boldsymbol{\Phi}_2 - \frac{\partial \alpha_2}{\partial x_2} \frac{\boldsymbol{\Phi}_1}{m}\| \cdot \|\boldsymbol{\theta}_M\| + \delta_2(t) + \frac{\delta_1(t)}{m} \left| \frac{\partial \alpha_2}{\partial x_2} \right| \right\}. \quad (94)$$

B. For a limited period of time, $\tilde{\Delta}_1 = \tilde{\Delta}_2 = 0$, asymptotic tracking performance can also be got, i.e., $z_1 \to 0$ as $t \to \infty$.

The proofs of Theorems 6.1 and 6.2 are a little complex, for more details, please see Ref. [23].

3.6.3 Experimental verification

In order to prove the usefulness of the developed nonlinear adaptive repetitive controller (APC), experimental results were obtained in Ref. [23] by comparing APC controller with the other three controllers, i.e., PID controller, ARC controller and feedback linearization controller (FLC). Some indexes are used to assess the performance of the control algorithm: The maximal value of tracking error M_e, the average value of tracking error μ, the standard deviation value of the tracking error σ defined in Ref. [23]. To test the performance of four controllers, a normal-level sinusoidal-like periodic trajectory $x_{1d} = 10(1-\cos(3.14t))(1-\exp(-t))^\circ$ was used. The tracking perfor-

mances of four controllers are presented in Fig. 12. Table 2 presents the tracking performance indices of four controllers during the last three cycles. Figure 13 shows the parameter adaptation of APC controller for normal motion. To further test the control scheme of the proposed algorithm in all work conditions, a fast motion trajectory x_{1d}= 10(1–cos(12.56t))(1–exp(–t))° was used. For the fast motion case, the tracking errors of APC and ARC controllers are given in Fig. 14, and the performance indices were summarized in Table 3. All results demonstrate that the developed nonlinear adaptive repetitive controller achieves a better performance than the other controllers. The reader can get more details about the experiments in Ref. [23].

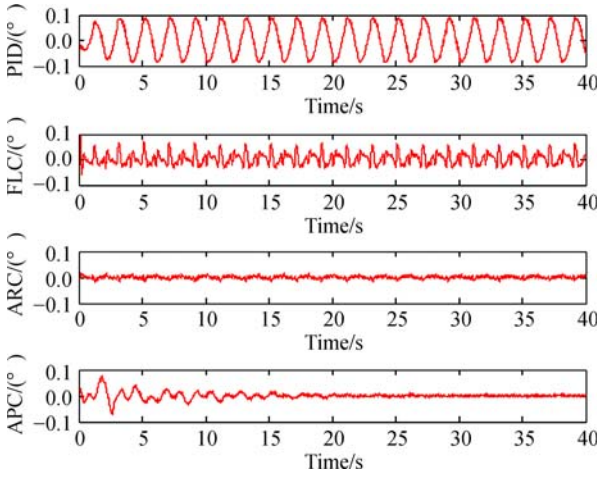

Fig. 12 Tracking errors of APC, ARC, FLC and PID for normal motion

Table 2 Performance indices for normal tracking case

Indices	M_e	μ	σ
PID	0.0896	0.0532	0.0274
FLC	0.0637	0.0198	0.0125
ARC	0.0136	0.0035	0.0026
APC	0.0089	0.0016	0.0012

3.7 Nonlinear friction compensation

As described in Case 7, The traditional piecewise continuous LuGre model cannot be utilized in the backstepping design for hydraulic control. Hence, a new continuously differentiable LuGre friction model for hydraulic system is developed in Ref. [24], which is given as follows:

$$\begin{cases} \dot{z} = \omega - N(\omega)z \\ f_r(t) = \sigma_0 z + \sigma_1 \dot{z} + \sigma_2 \omega \end{cases}, \quad (95)$$

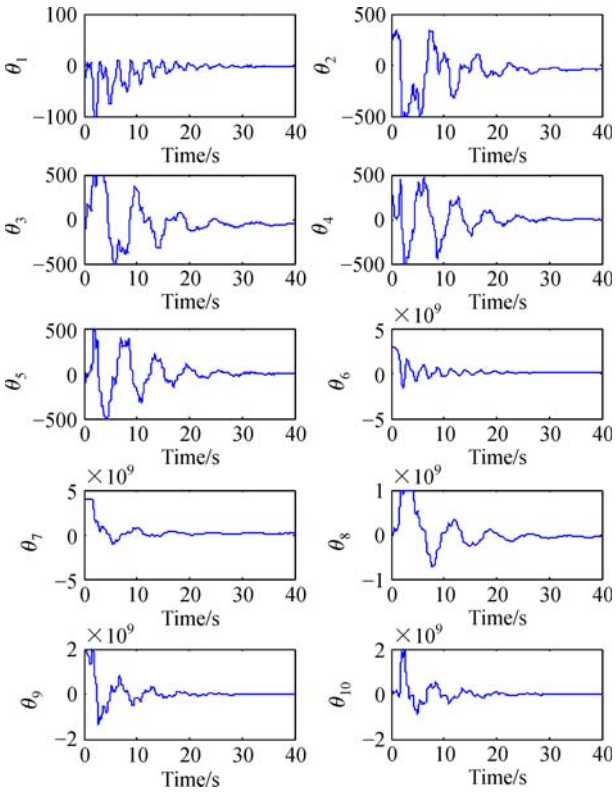

Fig. 13 Parameter estimation of APC for normal motion

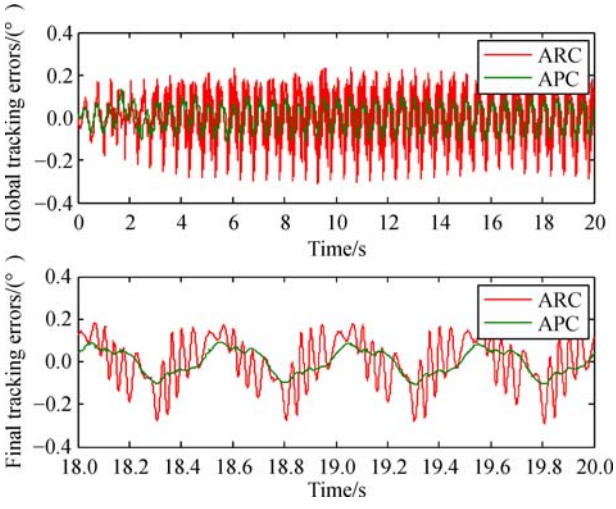

Fig. 14 Tracking errors of ARC and APC controllers for fast motion

Table 3 Performance indices for fast tracking case

Indices	M_e	μ	σ
ARC	0.2899	0.0935	0.0623
APC	0.1084	0.0517	0.0244

where σ_0 represents the stiffness of the bristles, σ_1 represents damping coefficient of the bristles, σ_2 represents the viscous coefficient, ω represents the angular velocity, z represents the internal unmeasurable friction state which means the average deflection of the bristles, $N(\omega)=\omega/g(\omega)$, in which $g(\omega)$ represents the static friction force defined as

$$g(\omega) = (f_s - f_c)[\tanh(c_1\omega) - \tanh(c_2\omega)] + f_c\tanh(c_3\omega), \tag{96}$$

where f_c represents the Coulomb friction and f_s represents the stiction friction.

In addition, for this case, the internal leakage model is given by

$$q_L = C_t P_L + C_s\sqrt{|P_L|}\text{sign}(P_L), \tag{97}$$

where C_t and C_s represent the contraction coefficients for round and slot type orifices.

The state variables are chosen as $\boldsymbol{x}=[x_1, x_2, x_3]^T=[y, \dot{y}, P_L]^T$, and with the friction and internal leakage model, the entire system dynamic can be expressed as

$$\begin{cases} \dot{z} = x_2 - N(x_2)z \\ \dot{x}_1 = x_2 \\ m\dot{x}_2 = Ax_3 - \sigma_0 z + \sigma_1 N(x_2)z - (\sigma_1+\sigma_2)x_2 - f_e(t) \\ \dot{x}_3 = \beta_e k_t f_1 u - \beta_e f_2 - \beta_e C_t f_3 - \beta_e C_s f_4 - q(t) \end{cases}, \tag{98}$$

where f_1, f_2, f_3 and f_4 are known nonlinear functions defined by

$$f_1 = \frac{R_1}{V_1} + \frac{R_2}{V_2},\ f_2 = \left(\frac{1}{V_1} + \frac{1}{V_2}\right)Ax_2,$$
$$f_3 = \left(\frac{1}{V_1} + \frac{1}{V_2}\right)x_3,\ f_4 = \left(\frac{1}{V_1} + \frac{1}{V_2}\right)\sqrt{|x_3|}\text{sign}(x_3). \tag{99}$$

The unknown parameter set was defined as $\boldsymbol{\theta} = [\theta_1, \theta_2, \theta_3, \theta_4, \theta_5, \theta_6, \theta_7, \theta_8, \theta_9, \theta_{10}]^T$, where $\theta_1=\sigma_0$, $\theta_2=\sigma_1$, $\theta_3=\sigma_1+\sigma_2$, $\theta_4=d_n$, $\theta_5=\beta_e k_t$, $\theta_6=\beta_e$, $\theta_7=\beta_e C_t$, $\theta_8=\beta_e k_t u_0$, $\theta_9=q_n$, and $\theta_{10}=\beta_e C_s$. Thus, the state-space form can be formulated as

$$\begin{cases} \dot{z} = x_2 - N(x_2)z \\ \dot{x}_1 = x_2 \\ m\dot{x}_2 = Ax_3 - \theta_1 z + \theta_2 N(x_2)z - \theta_3 x_2 - \theta_4 + \tilde{d}(t) \\ \dot{x}_3 = \theta_5 f_1 u - \theta_6 f_2 - \theta_7 f_3 - \theta_8 f_1 - \theta_9 - \theta_{10} f_4 + \tilde{q}(t) \end{cases}, \tag{100}$$

where $\tilde{d}(t)\triangleq d_n - f_e(t)$, $\tilde{q}(t)\triangleq q_n - q(t)$ represent the time-variant modelling errors existed in Eq. (100).

Just as the parameter set $\boldsymbol{\theta}$ is unknown. the internal friction state z in Eq. (95) is also unknown. Therefore, it is necessary to construct an observation scheme for the unknown state z in the nonlinear controller design. Note that two different terms $\theta_1 z$ and $\theta_2 N(x_2)z$ have a relationship with the state z. In order to construct an observation scheme for z, robust observers with dual-observer structure were proposed in Refs. [25,26]:

$$\dot{\hat{z}}_1 = \text{Proj}_{\hat{z}_1}(\eta_1),\ \ \dot{\hat{z}}_2 = \text{Proj}_{\hat{z}_2}(\eta_2), \tag{101}$$

where $\hat{z}_1$ and $\hat{z}_2$ represent the estimation of state z, η_1 and η_2 will be designed later, the projection mapping in Eq. (101) is expressed as:

$$\text{Proj}_{\hat{z}_i}(\eta_i) = \begin{cases} 0 & \text{if } \hat{z}_i = z_{\max} \text{ and } \eta_i > 0 \\ 0 & \text{if } \hat{z}_i = z_{\min} \text{ and } \eta_i < 0 \\ \eta_i & \text{otherwise} \end{cases} \tag{102}$$

where the bounds for observation can be set as $z_{\max}=f_s$, $z_{\min}=-f_s$ [25], which are related to the physical bounds of the friction state z.

As with the parameter adaptation, for any chosen functions η_1 and η_2, the projection mapping defined in Eq. (101) ensures [25]

$$\textbf{P3}: \begin{cases} z_{1\min} \leqslant \hat{z}_1 \leqslant z_{1\max} \\ z_{2\min} \leqslant \hat{z}_2 \leqslant z_{2\max}, \end{cases} \tag{103}$$

$$\textbf{P4}: \begin{cases} \tilde{z}_1(\dot{\hat{z}}_1 - \eta_1) \leqslant 0 \\ \tilde{z}_2(\dot{\hat{z}}_2 - \eta_2) \leqslant 0, \end{cases} \tag{104}$$

where $\tilde{z}_1 = \hat{z}_1 - z$ and $\tilde{z}_2 = \hat{z}_2 - z$ represent the estimation errors, and the dynamics of the errors can be expressed as

$$\begin{cases} \dot{\tilde{z}}_1 = \dot{\hat{z}}_1 - \dot{z} = \text{Proj}_{\hat{z}_1}(\eta_1) - [x_2 - N(x_2)z] \\ \dot{\tilde{z}}_2 = \dot{\hat{z}}_2 - \dot{z} = \text{Proj}_{\hat{z}_2}(\eta_2) - [x_2 - N(x_2)z] \end{cases}. \tag{105}$$

3.7.1 Adaptive controller design with nonlinear friction compensation

Define the error variables similar to Eq. (16),

$$e_1 = x_1 - x_{1d},\ e_2 = \dot{e}_1 + k_1 e_1 = x_2 - \alpha_1,$$
$$\alpha_1 \triangleq \dot{x}_{1d} - k_1 e_1,\ e_3 = x_3 - \alpha_2. \tag{106}$$

Note the system model Eq. (100), the error dynamics can be written as

$$m\dot{e}_2 = Ax_3 - m\dot{\alpha}_1 - \theta_1 z + \theta_2 N(x_2)z - \theta_3 x_2 - \theta_4 + \tilde{d}(t),$$
$$\dot{e}_3 = \theta_5 f_1 u - \theta_6 f_2 - \theta_7 f_3 - \theta_8 f_1 - \theta_9 - \theta_{10} f_4 - \dot{\alpha}_2 + \tilde{q}(t). \tag{107}$$

Based on the backstepping design procedure, the virtual control law α_2 and the adaptive control law u and can be

designed as

$$\alpha_2 = \frac{1}{A}(\alpha_{2a} + \alpha_{2s}),$$

$$\alpha_{2a} = m\dot{\alpha}_1 + \hat{\theta}_1\hat{z}_1 - \hat{\theta}_2 N(x_2)\hat{z}_2 + \hat{\theta}_3 x_2 + \hat{\theta}_4,$$

$$\alpha_{2s} = \alpha_{2s1} + \alpha_{2s2},$$

$$\alpha_{2s1} = -k_2 e_2,$$

$$\alpha_{2s2} = -k_{s2}e_2 \triangleq -\frac{h_2+1}{4\varepsilon_2}e_2, \tag{108}$$

$$u = u_a + u_s,$$

$$u_a = \frac{1}{\hat{\theta}_5 f_1}\left(\hat{\theta}_6 f_2 + \hat{\theta}_7 f_3 + \hat{\theta}_8 f_1 + \hat{\theta}_9 + \hat{\theta}_{10} f_4 + \dot{\alpha}_2\right),$$

$$u_s = \frac{1}{\theta_{5\min} f_1}(u_{s1} + u_{s2}),$$

$$u_{s1} = -k_3 e_3,$$

$$u_{s2} = -k_{s3}e_3 \triangleq -\frac{h_3+1}{4\varepsilon_3}e_3, \tag{109}$$

where ε_2 and ε_3 are positive constants, k_{s2} and k_{s3} are positive nonlinear gains, and h_2 and h_3 are smooth functions satisfying

$$h_2 \geqslant [\|\boldsymbol{\theta}_M\|\|\boldsymbol{\varphi}_2\| + \theta_{1M}z_M + \theta_{2M}N(x_2)z_M]^2,$$

$$h_3 \geqslant \|\boldsymbol{\theta}_M\|^2\|\boldsymbol{\varphi}_3\|^2, \tag{110}$$

in which $\boldsymbol{\theta}_M = \boldsymbol{\theta}_{max} - \boldsymbol{\theta}_{min}$, $\theta_{1M} = \theta_{1max} - \theta_{1min}$, $\theta_{2M} = \theta_{2max} - \theta_{2min}$, $z_M = z_{max} - z_{min}$.

Substituting the virtual control α_2 and the actual control input u into the error dynamics Eq. (107), it can be obtained

$$m\dot{e}_2 = Ae_3 - k_2 e_2 + \alpha_{2s2} - \tilde{\boldsymbol{\theta}}^T\boldsymbol{\varphi}_2 + \theta_1\tilde{z}_1 - \theta_2 N(x_2)\tilde{z}_2 + \tilde{d}(t), \tag{111}$$

$$\dot{e}_3 = -\frac{\theta_5}{\theta_{5\min}}k_3 e_3 + \frac{\theta_5}{\theta_{5\min}}u_{s2} - \tilde{\boldsymbol{\theta}}^T\boldsymbol{\varphi}_3 + \tilde{q}(t), \tag{112}$$

where $\boldsymbol{\varphi}_2 \triangleq [-\hat{z}_1, N(x_2)\hat{z}_2, -x_2, -1, 0, 0, 0, 0, 0, 0]^T$ and $\boldsymbol{\varphi}_3 \triangleq [0,0,0,0,f_1 u_a, -f_2, -f_3, -f_1, -1, -f_4]^T$ are regressors for parameter adaptation.

3.7.2 Stability analysis

Theorem 7: As the adaptation law mentioned in Eq. (46) and the adaptation function $\boldsymbol{\tau} = \boldsymbol{\varphi}_2 z_2 + \boldsymbol{\varphi}_3 z_3$, the friction state observation Eq. (101) and learning functions expressed as

$$\begin{cases} \eta_1 = x_2 - N(x_2)\hat{z}_1 - \gamma_1 e_2 \\ \eta_2 = x_2 - N(x_2)\hat{z}_2 + \gamma_2 N(x_2)e_2 \end{cases}, \tag{113}$$

where γ_1 and γ_2 are learning gains, and the control gain k_1, k_2, and k_3 are defined sufficiently large, so the matrix $\boldsymbol{\Lambda}_1$ defined in Eq. (20) can be guaranteed to be positive definite., the designed adaptive control with nonlinear friction compensation guarantees that:

A. If there does not exist time-variant modelling errors in the system, i.e., $\tilde{d} = \tilde{q} = 0$, there only exists parametric uncertainties and nonlinear frictions in the system, all system signals are in a bounded range, and can also get asymptotic tracking performance, i.e., $e_1 \to 0$ as $t \to \infty$.

B. If the time-variant modelling errors does exist in the system, i.e., $\tilde{d} \neq \tilde{q} \neq 0$, then the control law Eq. (38) ensures that all system signals are in a bounded range under closed-loop operation, and the upper bound of Lyapunov function $V_1(t)$ defined in Eq. (21) can be expressed as

$$V_1(t) \leqslant V_1(0)\exp(-\kappa t) + \varepsilon\frac{1 + \|\delta(t)\|_\infty}{\kappa}[1 - \exp(-\kappa t)], \tag{114}$$

where $\varepsilon = \varepsilon_2 + \varepsilon_3$, and $\kappa \triangleq 2\lambda_{\min}(\boldsymbol{\Lambda}_1)\min\{1, 1/m, 1\}$, $\delta(t) \triangleq \max\{\delta_1^2(t), \delta_2^2(t)\}$.

Proof: First consider the proof of Part A, a positive Lyapunov function is defined as

$$V_3 = \frac{1}{2}e_1^2 + \frac{1}{2}me_2^2 + \frac{1}{2}e_3^2 + \frac{1}{2}\tilde{\boldsymbol{\theta}}^T\boldsymbol{\Gamma}^{-1}\tilde{\boldsymbol{\theta}} + \frac{1}{2}\theta_1\gamma_1^{-1}\tilde{z}_1^2 + \frac{1}{2}\theta_2\gamma_2^{-1}\tilde{z}_2^2. \tag{115}$$

The time derivative of V_3 is

$$\begin{aligned}\dot{V}_3 &= e_1\dot{e}_1 + me_2\dot{e}_2 + e_3\dot{e}_3 + \tilde{\boldsymbol{\theta}}^T\boldsymbol{\Gamma}^{-1}\dot{\hat{\boldsymbol{\theta}}} + \gamma_1^{-1}\theta_1\tilde{z}_1\dot{\tilde{z}}_1 + \gamma_2^{-1}\theta_2\tilde{z}_2\dot{\tilde{z}}_2 \\ &= -k_1e_1^2 + e_1e_2 - (k_2 + k_{s2})e_2^2 + Ae_2e_3 - \frac{\theta_5}{\theta_{5\min}}(k_3 + k_{s3})e_3^2 + \tilde{\boldsymbol{\theta}}^T\boldsymbol{\Gamma}^{-1}\dot{\hat{\boldsymbol{\theta}}} \\ &\quad - \tilde{\boldsymbol{\theta}}^T\boldsymbol{\varphi}_2e_2 - \tilde{\boldsymbol{\theta}}^T\boldsymbol{\varphi}_3e_3 + \gamma_1^{-1}\theta_1\tilde{z}_1\dot{\tilde{z}}_1 + \gamma_2^{-1}\theta_2\tilde{z}_2\dot{\tilde{z}}_2 + \theta_1\tilde{z}_1e_2 - \theta_2N(x_2)\tilde{z}_2e_2 \\ &\leqslant -k_1e_1^2 + e_1e_2 - k_2e_2^2 + Ae_2e_3 - k_3e_3^2 + \gamma_1^{-1}\theta_1\tilde{z}_1\dot{\tilde{z}}_1 + \gamma_2^{-1}\theta_2\tilde{z}_2\dot{\tilde{z}}_2 + \theta_1\tilde{z}_1e_2 - \theta_2N(x_2)\tilde{z}_2e_2.\end{aligned} \tag{116}$$

Note that the matrix $\boldsymbol{\Lambda}_1$ is positive definite, and with the dynamics expressed in Eq. (105), we can get

$$\dot{V}_3 \leqslant -\boldsymbol{e}^{\mathrm{T}}\boldsymbol{\Lambda}\boldsymbol{e} + \gamma_1^{-1}\theta_1\tilde{z}_1[\dot{\hat{z}}_1 - x_2 + N(x_2)\hat{z}_1 + \gamma_1 e_2] + \gamma_2^{-1}\theta_2\tilde{z}_2[\dot{\hat{z}}_2 - x_2 + N(x_2)\hat{z}_2 - \gamma_2 N(x_2)e_2] - \gamma_1^{-1}\theta_1 N(x_2)\tilde{z}_1^2 - \gamma_2^{-1}\theta_2 N(x_2)\tilde{z}_2^2. \quad (117)$$

Combing the definition of η_1 and η_2 in Eq. (113), the property in Eq. (104), and noting that the positive nonlinear function $N(x_2)$, the upper bound of the above equation can be expressed as

$$\dot{V}_3 \leqslant -\boldsymbol{e}^{\mathrm{T}}\boldsymbol{\Lambda}_1\boldsymbol{e} - \gamma_1^{-1}\theta_1 N(x_2)\tilde{z}_1^2 - \gamma_2^{-1}\theta_2 N(x_2)\tilde{z}_2^2 \leqslant -\boldsymbol{e}^{\mathrm{T}}\boldsymbol{\Lambda}_1\boldsymbol{e} \leqslant -\lambda_{\min}(\boldsymbol{\Lambda}_1)(e_1^2 + e_2^2 + e_3^2) \triangleq -W_4. \quad (118)$$

Based on Barbalat's lemma, $W_4 \to 0$ as $t \to \infty$, which derives the Part A of Theorem 7. Then consider the proof of part B, the time derivative of $V_1(t)$ can be expressed as

$$\begin{aligned}\dot{V}_1 =& -k_1 e_1^2 + e_1 e_2 - (k_2 + k_{s2})e_2^2 + Ae_2 e_3 - \frac{\theta_5}{\theta_{5\min}}(k_3 + k_{s3})e_3^2 \\ & - \tilde{\boldsymbol{\theta}}^{\mathrm{T}}\boldsymbol{\varphi}_2 e_2 + \theta_1\tilde{z}_1 e_2 - \theta_2 N(x_2)\tilde{z}_2 e_2 \\ & + \tilde{d}(t)e_2 - \tilde{\boldsymbol{\theta}}^{\mathrm{T}}\boldsymbol{\varphi}_3 e_3 + \tilde{q}(t)e_3 \\ \leqslant& -k_1 e_1^2 + e_1 e_2 - k_2 e_2^2 + Ae_2 e_3 - k_3 e_3^2 \\ & - \frac{h_2}{4\varepsilon_2}e_2^2 - e_2\left[\tilde{\boldsymbol{\theta}}^{\mathrm{T}}\boldsymbol{\varphi}_2 - \theta_1\tilde{z}_1 + \theta_2 N(x_2)\tilde{z}_2\right] \\ & - \frac{1}{4\varepsilon_2}e_2^2 + \tilde{d}(t)e_2 - \frac{h_3}{4\varepsilon_3}e_3^2 \\ & - \tilde{\boldsymbol{\theta}}^{\mathrm{T}}\boldsymbol{\varphi}_3 e_3 - \frac{1}{4\varepsilon_3}e_3^2 + \tilde{q}(t)e_3. \end{aligned} \quad (119)$$

Based on the condition of h_2, the upper bound of the second term of above inequality can be summarized as

$$-\frac{h_2 e_2^2}{4\varepsilon_2} - e_2\left[\tilde{\boldsymbol{\theta}}^{\mathrm{T}}\boldsymbol{\varphi}_2 - \theta_1\tilde{z}_1 + \theta_2 N(x_2)\tilde{z}_2\right] - \frac{e_2^2}{4\varepsilon_2} + e_2\tilde{d}(t) \leqslant \varepsilon_2 + \varepsilon_2\delta_1^2(t). \quad (120)$$

Similarly,

$$-\frac{h_3}{4\varepsilon_3}e_3^2 - \tilde{\boldsymbol{\theta}}^{\mathrm{T}}\boldsymbol{\varphi}_3 e_3 - \frac{1}{4\varepsilon_3}e_3^2 + \tilde{q}(t)e_3 \leqslant \varepsilon_3 + \varepsilon_3\delta_2^2(t). \quad (121)$$

Thus,

$$\begin{aligned}\dot{V}_1 &\leqslant -\boldsymbol{e}^{\mathrm{T}}\boldsymbol{\Lambda}\boldsymbol{e} + \varepsilon + \varepsilon_2\delta_1^2(t) + \varepsilon_3\delta_2^2(t) \\ &\leqslant -\lambda_{\min}(\boldsymbol{\Lambda})(e_1^2 + e_2^2 + e_3^2) + \varepsilon + \varepsilon\delta(t) \\ &\leqslant -\kappa V + \varepsilon + \varepsilon\delta(t). \end{aligned} \quad (122)$$

By employing the Comparing lemma [3], it can be concluded that $V_1(t)$ can be upper bounded by Eq. (114).

3.7.3 Experimental verification

In order to prove the usefulness of the designed nonlinear adaptive controller with modified LuGre model based friction compensation (ALuGre), the experimental results presented below were obtained in Ref. [24] The ALuGre controller was compared with the nonlinear adaptive controller (AC), the FLC, and PI controller with velocity feedforward (VFPI). To test the performance of four controllers, a smooth normal motion trajectory $x_{1\mathrm{d}} = 10(1-\cos(3.14t))(1-\exp(-t))^\circ$ was used. The tracking performances of four controllers are presented in Figs. 15 and 16, the performance indices during the last two cycles are summarized in Table 4. To further test the control scheme of the proposed friction compensation algorithm, a slow motion trajectory $x_{1\mathrm{d}} = 10(1-\cos(0.628t))(1-\exp(-t))^\circ$ was used. For the slow motion case, the comparative tracking performance and performance indices are given in Figs. 17 and 18, and Table 5. It can be observed from the presented experimental results that the developed ALuGre controller handles better than the

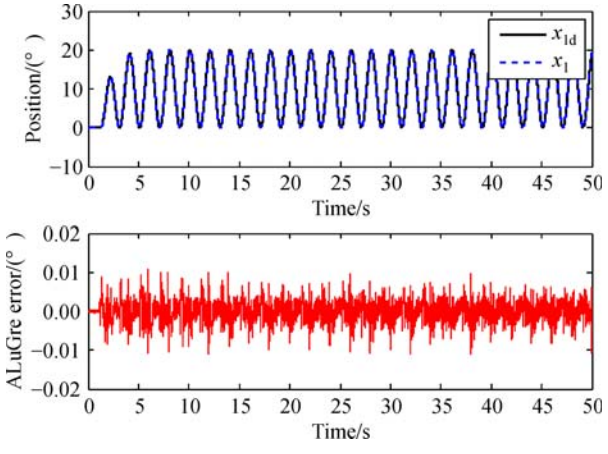

Fig. 15 Tracking performance of ALuGre for normal motion

Table 4 Performance indices in normal tracking case

Indices	M_e	μ	σ
PIVF	0.0903	0.0531	0.0274
FLC	0.0663	0.0200	0.0132
AC	0.0123	0.0030	0.0024
ALuGre	0.0081	0.0019	0.0015

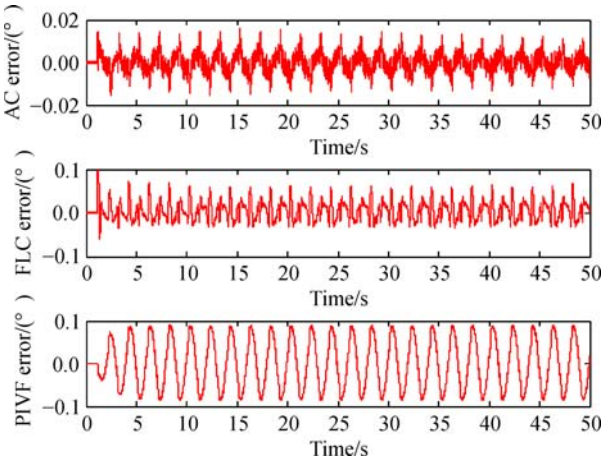

Fig. 16 Tracking errors of the other three controllers for normal motion

Table 5 Performance indices in slow tracking case

Indices	M_e	μ	σ
PIVF	0.0213	0.0044	0.0047
FLC	0.0414	0.0050	0.0092
AC	0.0125	0.0013	0.0016
ALuGre	0.0041	0.0008	0.0006

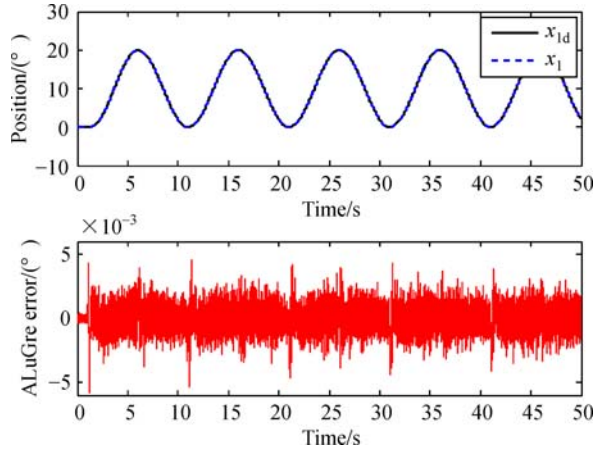

Fig. 17 Tracking performance of ALuGre for slow motion

other three controllers considering both transient and steady-state tracking performance, which demonstrate the effectiveness of the proposed modified LuGre friction model and the adaptive control method. The reader can get more details about the experiments in Ref. [24].

3.8 Nonlinear output feedback control

In Case 8, only output measurement of the hydraulic

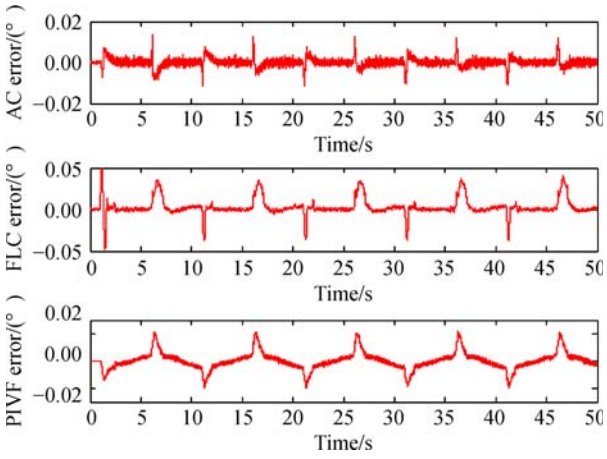

Fig. 18 Tracking errors of the other three controllers for slow motion

system is available. Hence, nonlinear output feedback control is developed in this section. From the physical model Eqs. (1), (7)–(10), choose the state variables as $\boldsymbol{x}=[x_1, x_2, x_3]^{\mathrm{T}}=[y, \dot{y}, AP_{\mathrm{L}}/m]^{\mathrm{T}}$, Then the system model for this case is given as

$$\begin{cases} \dot{x}_1 = x_2 \\ \dot{x}_2 = x_3 + \phi_1(x_2) + d(t) \\ \dot{x}_3 = g(u,x_3)u + \phi_2(x_2,x_3) + q_{\mathrm{o}} + q(t) \end{cases}, \tag{123}$$

where $\phi_1(x_2) = -F(x_2)/J$, $d(t) = f(t,x_1,x_2)/J$, $q_{\mathrm{o}} = 4\beta_{\mathrm{e}}D_{\mathrm{m}}Q_{\mathrm{o}}/(V_{\mathrm{t}}J)$, $q(t) = 4\beta_{\mathrm{e}}D_{\mathrm{m}}Q(t)/(V_{\mathrm{t}}J)$ and

$$g(u,x_3) = \frac{4D_{\mathrm{m}}\beta_{\mathrm{e}}k_{\mathrm{t}}}{JV_{\mathrm{t}}}\sqrt{P_{\mathrm{s}} - \mathrm{sign}(u)\frac{J}{D_{\mathrm{m}}}x_3},$$

$$\phi_2(x_2,x_3) = -\frac{4D_{\mathrm{m}}^2\beta_{\mathrm{e}}}{JV_{\mathrm{t}}}x_2 - \frac{4\beta_{\mathrm{e}}}{V_{\mathrm{t}}}C_{\mathrm{t}}x_3. \tag{124}$$

In the observer-controller design below, the nominal values of the physical parameters can be utilized, and the parameter deviations are included in the unmodeled terms, i.e., $d(t)$ and q_{o}, $q(t)$ in Eq. (123). Before the observer design, at first the major modeling uncertainty $q_{\mathrm{o}}+q(t)$ was extended as an additional state variable, i.e., define $x_4 = q_{\mathrm{o}}+q(t)$, and the system state is changed to $\boldsymbol{x}=[x_1, x_2, x_3, x_4]^{\mathrm{T}}$. The time derivative of x_4 was represented by $h(t)$. then the original plant in Eq. (123) can be rewrote as

$$\begin{cases} \dot{x}_1 = x_2 \\ \dot{x}_2 = x_3 + \phi_1(x_2) + d(t) \\ \dot{x}_3 = g(u,x_3)u + \phi_2(x_2,x_3) + x_4 \\ \dot{x}_4 = h(t) \end{cases}. \tag{125}$$

Assumption 7: The function $g(u, x_3)$ is Lipschitz related to x_3 within its practical range; $\phi_1(x_2)$ is globally Lipschitz

related to x_2; and $\phi_2(x_2, x_3)$ is Lipschitz related to x_2 and x_3.

3.8.1 Nonlinear output feedback controller design

To estimate the unmeasurable states (i.e., x_2, x_3) and the modeling uncertainty x_4, a linear extended state observer (LESO) in Ref. [27] is constructed. Define $\hat{\boldsymbol{x}}$ as the estimate of $\boldsymbol{x}$ and $\tilde{\boldsymbol{x}}$ as the estimation error (i.e., $\tilde{\boldsymbol{x}} = \boldsymbol{x} - \hat{\boldsymbol{x}}$). Firstly, the extended system model Eq. (125) can be rewritten as

$$\begin{cases} \dot{\boldsymbol{x}} = \boldsymbol{A}_{\mathrm{o}}\boldsymbol{x} + \boldsymbol{\Phi}(\boldsymbol{x}) + \boldsymbol{G}(u,\boldsymbol{x})u + \boldsymbol{\Delta}(t) \\ \boldsymbol{y} = \boldsymbol{C}\boldsymbol{x} \end{cases}, \tag{126}$$

where

$$\boldsymbol{A}_{\mathrm{o}} = \begin{bmatrix} 0 & 1 & 0 & 0 \\ 0 & 0 & 1 & 0 \\ 0 & 0 & 0 & 1 \\ 0 & 0 & 0 & 0 \end{bmatrix}, \ \boldsymbol{\Phi}(x) = \begin{bmatrix} 0 \\ \phi_1(x_2) \\ \phi_2(x_2,x_3) \\ 0 \end{bmatrix},$$

$$\boldsymbol{G}(u,x) = \begin{bmatrix} 0 \\ 0 \\ g(u,x_3) \\ 0 \end{bmatrix}, \ \boldsymbol{\Delta}(t) = \begin{bmatrix} 0 \\ d(t) \\ 0 \\ h(t) \end{bmatrix}, \boldsymbol{C} = \begin{bmatrix} 1 \\ 0 \\ 0 \\ 0 \end{bmatrix}.$$

Then based on Eq. (126), the LESO can be constructed as

$$\dot{\hat{\boldsymbol{x}}} = \boldsymbol{A}_{\mathrm{o}}\hat{\boldsymbol{x}} + \boldsymbol{\Phi}(\hat{\boldsymbol{x}}) + \boldsymbol{G}(u,\hat{\boldsymbol{x}})u + \boldsymbol{H}(x_1 - \hat{x}_1), \tag{127}$$

where $\boldsymbol{\Phi}(\hat{\boldsymbol{x}}) = [0, \ \phi_1(\hat{\boldsymbol{x}}_2), \ \phi_2(\hat{\boldsymbol{x}}_2,\hat{\boldsymbol{x}}_3), \ 0]^{\mathrm{T}}$, $\boldsymbol{G}(u,\hat{\boldsymbol{x}}) = [0, \ 0, \ g(u,\hat{\boldsymbol{x}}_3), \ 0]^{\mathrm{T}}$ and $\boldsymbol{H}$ is the observer gain given by $\boldsymbol{H} = [4\omega_{\mathrm{o}}, \ 6\omega_{\mathrm{o}}^2, \ 4\omega_{\mathrm{o}}^3, \ \omega_{\mathrm{o}}^4]^{\mathrm{T}}$, in which $\omega_{\mathrm{o}} > 0$ representing the bandwidth of the observer is the only tuning parameter.

From Eqs. (126) and (127), the differential of the state estimation error can be given as

$$\dot{\tilde{\boldsymbol{x}}} = \boldsymbol{A}_{\mathrm{o}}\tilde{\boldsymbol{x}} + \boldsymbol{\Phi}(\boldsymbol{x}) - \boldsymbol{\Phi}(\hat{\boldsymbol{x}}) + [\boldsymbol{G}(u,\boldsymbol{x}) - \boldsymbol{G}(u,\hat{\boldsymbol{x}})]u - \boldsymbol{H}\tilde{x}_1 + \boldsymbol{\Delta}(t). \tag{128}$$

Define

$$\tilde{\phi}_1 \triangleq \phi_1(x_2) - \phi_1(\hat{x}_2), \ \tilde{g} \triangleq g(u,x_3) - g(u,\hat{x}_3),$$

$$\tilde{\phi}_2 \triangleq \phi_2(x_2,x_3) - \phi_2(\hat{x}_2,\hat{x}_3), \tag{129}$$

and define the scaled estimation error as $\varepsilon_i = \tilde{x}_i/\omega_{\mathrm{o}}^{i-1}$, $i =$ 1, 2, 3, and 4, then Eq. (128) can be rewrote as

$$\dot{\boldsymbol{\varepsilon}} = \omega_{\mathrm{o}}\boldsymbol{A}\boldsymbol{\varepsilon} + \boldsymbol{B}_2\frac{\tilde{\varphi}_1 + d(t)}{\omega_{\mathrm{o}}} + \boldsymbol{B}_3\frac{(\tilde{\varphi}_2 + \tilde{g}u)}{\omega_{\mathrm{o}}^2} + \boldsymbol{B}_4\frac{h(t)}{\omega_{\mathrm{o}}^3}, \tag{130}$$

where $\boldsymbol{\varepsilon} = [\varepsilon_1, \ \varepsilon_2, \ \varepsilon_3, \ \varepsilon_4]^{\mathrm{T}}$ and

$$\boldsymbol{A} = \begin{bmatrix} -4 & 1 & 0 & 0 \\ -6 & 0 & 1 & 0 \\ -4 & 0 & 0 & 1 \\ -1 & 0 & 0 & 0 \end{bmatrix}, \ \boldsymbol{B}_2 = \begin{bmatrix} 0 \\ 1 \\ 0 \\ 0 \end{bmatrix},$$

$$\boldsymbol{B}_3 = \begin{bmatrix} 0 \\ 0 \\ 1 \\ 0 \end{bmatrix}, \ \boldsymbol{B}_4 = \begin{bmatrix} 0 \\ 0 \\ 0 \\ 1 \end{bmatrix}, \tag{131}$$

in which $\boldsymbol{A}$ is Hurwitz. Thus, a positive definite matrix $\boldsymbol{P}$ exists so that the following Lyapunov equation holds

$$\boldsymbol{A}^{\mathrm{T}}\boldsymbol{P} + \boldsymbol{P}\boldsymbol{A} = -2\boldsymbol{I}. \tag{132}$$

Define the error variables as in Eq. (16), and note the extended system model in Eq. (125), the virtual control law α_2 and the proposed nonlinear output feedback controller u and can be given as

$$\alpha_2 = -\phi_1(\hat{x}_2) + \ddot{x}_{1\mathrm{d}} - k_1\hat{x}_2 + k_1\dot{x}_{1\mathrm{d}} - k_2(\hat{x}_2 - \alpha_1), \tag{133}$$

$$u = \frac{1}{g(u,\hat{x}_3)}[-\phi_2(\hat{x}_2,\hat{x}_3) - \hat{x}_4 + \dot{\alpha}_{2\mathrm{c}} - k_3(\hat{x}_3 - \alpha_2)], \tag{134}$$

where

$$\dot{\alpha}_{2\mathrm{c}} = \frac{\partial\alpha_2}{\partial t} + \frac{\partial\alpha_2}{\partial x_1}\hat{x}_2 + \frac{\partial\alpha_2}{\partial\hat{x}_2}\dot{\hat{x}}_2. \tag{135}$$

Substituting the virtual control α_2 and the actual control input u into the dynamics of z_2 and z_3, then

$$\dot{z}_2 = z_3 - k_2z_2 + \tilde{\phi}_1 + \omega_{\mathrm{o}}(k_1 + k_2)\varepsilon_2 + d(t), \tag{136}$$

$$\dot{z}_3 = -k_3z_3 + \omega_{\mathrm{o}}^2k_3\varepsilon_3 + \tilde{g}u + \tilde{\phi}_2 + \omega_{\mathrm{o}}^3\varepsilon_4 - \omega_{\mathrm{o}}\frac{\partial\alpha_2}{\partial x_1}\varepsilon_2. \tag{137}$$

3.8.2 Stability analysis

From the definitions of $\phi_1(x_2)$, $g(u, x_3)$, $\phi_2(x_2, x_3)$, ε_2 and ε_3 and based on Assumption 7, c_1, c_2, c_3 and c_4 are some known constants so that the following formulas hold

$$\begin{cases} |\phi_1(x_2) - \phi_1(\hat{x}_2)| \leqslant c_1|\varepsilon_2| \\ |g(u,x_3) - g(u,\hat{x}_3)| \leqslant c_2|\varepsilon_3| \\ |\phi_2(x_2,x_3) - \phi_2(\hat{x}_2,\hat{x}_3)| \leqslant c_3|\varepsilon_2| + c_4|\varepsilon_3| \end{cases}. \tag{138}$$

A set of known constants was defined as

$$\begin{cases} \kappa = \dfrac{1}{\omega_o^2}(\omega_o c_1\delta_2 + c_3\delta_3 + c_4\delta_3 + c_2\delta_3|u|_{\max}) \\ \gamma_1 = k_1\omega_o + k_2\omega_o + c_1 \\ \gamma_2 = \omega_o^2 k_3 + c_2|u|_{\max} + c_4 \\ \gamma_3 = \omega_o|\dfrac{\partial\alpha_2}{\partial x_1}| + c_3 \\ \gamma_4 = \omega_o^3 \\ \zeta = \dfrac{1}{2}|d(t)|_{\max}^2 + \dfrac{\delta_2^2}{2\omega_o^2}|d(t)|_{\max}^2 + \dfrac{\delta_4^2}{2\omega_o^6}|h(t)|_{\max}^2 \end{cases}, \quad (139)$$

where δ_i=$\|PB_i\|$ (i=2,3,4), $|u|_{\max}$ denotes the maximum hardware constraint for the control input; and the following performance theorem has been achieved.

Theorem 8: Based on the designed LESO in Eq. (127) under the hypothesis that $h(t)$ and $d(t)$ are bounded, and choosing gains k_1, k_2, k_3 and ω_o properly so that the following defined matrix $\mathbf{\Lambda}_5$ is positive definite

$$\mathbf{\Lambda}_5 = \begin{bmatrix} \mathbf{\Lambda}_1 & \mathbf{0} & \mathbf{\Lambda}_2 \\ \mathbf{0} & \omega_o - \kappa - 1 & \mathbf{0} \\ \mathbf{\Lambda}_2^{\mathrm{T}} & \mathbf{0} & \mathbf{\Lambda}_3 \end{bmatrix}, \quad (140)$$

where $\mathbf{0}$ denotes zero vector with proper dimensions, and

$$\mathbf{\Lambda}_1 = \begin{bmatrix} k_1 & -\dfrac{1}{2} & 0 \\ -\dfrac{1}{2} & k_2 - \dfrac{1}{2} & -\dfrac{1}{2} \\ 0 & -\dfrac{1}{2} & k_3 \end{bmatrix},$$

$$\mathbf{\Lambda}_2 = \begin{bmatrix} 0 & 0 & 0 \\ -\dfrac{\gamma_1}{2} & 0 & 0 \\ -\dfrac{\gamma_3}{2} & -\dfrac{\gamma_2}{2} & -\dfrac{\gamma_4}{2} \end{bmatrix},$$

$$\mathbf{\Lambda}_3 = \begin{bmatrix} \omega_o - \kappa - 1 & 0 & 0 \\ 0 & \omega_o - \kappa - 1 & 0 \\ 0 & 0 & \omega_o - \kappa - 1 \end{bmatrix}, \quad (141)$$

then, the designed control strategy Eq. (134) guarantees:

A. When existing time-varying modeling uncertainties in the controlled systems, i.e., $q(t)\neq 0$ and $d(t) \neq 0$, the state estimation error ε and the tracking error Z defined by $\boldsymbol{Z}$=$[z_1, z_2, z_3]^{\mathrm{T}}$ are all bounded. Furthermore, the following select positive definite function V_4:

$$V_4 = \frac{1}{2}\boldsymbol{Z}^{\mathrm{T}}\boldsymbol{Z} + \frac{1}{2}\boldsymbol{\varepsilon}^{\mathrm{T}}\boldsymbol{P}\boldsymbol{\varepsilon}, \quad (142)$$

is bounded above by

$$V_4(t) \leqslant V_4(0)\exp(-\tau t) + \frac{\zeta}{\tau}[1-\exp(-\tau t)], \quad (143)$$

where $\tau = 2\lambda_{\min}(\mathbf{\Lambda}_5)\min\{1, 1/\lambda_{\max}(\boldsymbol{P})\}$ is the exponentially converging rate, in which $\lambda_{\max}(\cdot)$ and $\lambda_{\min}(\cdot)$ represent the maximum and minimum eigenvalues of a matrix respectively.

B. If after a finite time t_0, $q(t)$ = $d(t)$ = 0, i.e., there not exist time-varying modeling uncertainties, then, not only results in A can be obtained, but also asymptotic output tracking is achieved, i.e., $z_1 \to 0$ as $t \to \infty$.

Proof: First consider the proof of A, the time derivative of V_4 is

$$\begin{aligned} \dot{V}_4 = & -k_1 z_1^2 - k_2 z_2^2 - k_3 z_3^2 - \omega_o\|\boldsymbol{\varepsilon}\|^2 \\ & + z_1 z_2 + z_2 z_3 + \omega_o(k_1 + k_2)\boldsymbol{\varepsilon}_2 z_2 \\ & + \omega_o^2 k_3 \boldsymbol{\varepsilon}_3 z_3 + \omega_o^3 \boldsymbol{\varepsilon}_4 z_3 - \omega_o\frac{\partial\alpha_2}{\partial x_1}\boldsymbol{\varepsilon}_2 z_3 \\ & + \tilde{\phi}_1 z_2 + \tilde{g}u z_3 + \tilde{\phi}_2 z_3 + \frac{1}{\omega_o}\boldsymbol{\varepsilon}^{\mathrm{T}}\boldsymbol{P}B_2\tilde{\phi}_1 \\ & + \frac{1}{\omega_o^2}\boldsymbol{\varepsilon}^{\mathrm{T}}\boldsymbol{P}B_3(\tilde{\phi}_2 + \tilde{g}u) + z_2 d(t) \\ & + \boldsymbol{\varepsilon}^{\mathrm{T}}\boldsymbol{P}B_2\frac{d(t)}{\omega_o} + \boldsymbol{\varepsilon}^{\mathrm{T}}\boldsymbol{P}B_4\frac{h(t)}{\omega_o^3}. \end{aligned} \quad (144)$$

Based on inequality Eq. (138) and the definitions in Eq. (139), then:

$$\begin{aligned} \dot{V}_4 \leqslant & -k_1 z_1^2 - \left(k_2 - \frac{1}{2}\right)z_2^2 - k_3 z_3^2 \\ & - (\omega_o - \kappa - 1)\|\boldsymbol{\varepsilon}\|^2 + |z_1||z_2| + |z_2||z_3| \\ & + \gamma_1|\varepsilon_2||z_2| + \gamma_2|\varepsilon_3||z_3| + \gamma_3|\varepsilon_2||z_3| \\ & + \gamma_4|\varepsilon_4||z_3| + \zeta = -\boldsymbol{\eta}^{\mathrm{T}}\mathbf{\Lambda}\boldsymbol{\eta} + \zeta, \end{aligned} \quad (145)$$

where $\boldsymbol{\eta}$=$[|z_1|, |z_2|, |z_3|, |\varepsilon_1|, |\varepsilon_2|, |\varepsilon_3|, |\varepsilon_4|]^{\mathrm{T}}$. Note that the matrix $\mathbf{\Lambda}_5$ is positive definite, thus

$$\begin{aligned} \dot{V}_4 & \leqslant -\lambda_{\min}(\mathbf{\Lambda}_5)(\|z\|^2 + \|\varepsilon\|^2) + \zeta \\ & \leqslant -\lambda_{\min}(\mathbf{\Lambda}_5)\left(\|z\|^2 + \frac{1}{\lambda_{\max}(P)}\boldsymbol{\varepsilon}^{\mathrm{T}}\boldsymbol{P}\boldsymbol{\varepsilon}\right) + \zeta \\ & \leqslant -\tau V_4 + \zeta, \end{aligned} \quad (146)$$

which leads to Eq. (143) through utilizing Comparison Lemma [3]. Now for Part B, when $q(t)$= 0, it can be inferred that $h(t)$= 0 through the definition of x_4. Based on $d(t)$= 0 and Eq. (144), and using the identical upper bound method in the proof of A, thus

$$\dot{V}_4 \leqslant -\lambda_{\min}(\mathbf{\Lambda}_5)(\|\boldsymbol{z}\|^2 + \|\boldsymbol{\varepsilon}\|^2) \triangleq -W_5. \quad (147)$$

Through utilizing Barbalat's lemma, $W_5 \to 0$ as $t \to \infty$, which leads to the Part B of Theorem 8.

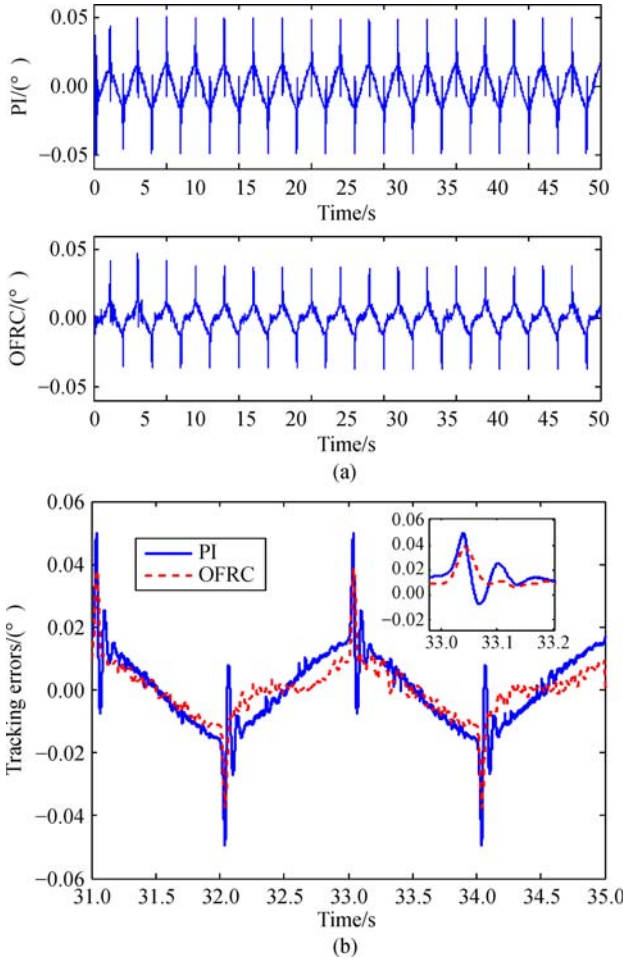

Fig. 19 Tracking errors of OFRC and PI controllers in normal case. (a) Tracking errors during the whole period in normal case; (b) tracking errors during the last two cycles in normal case

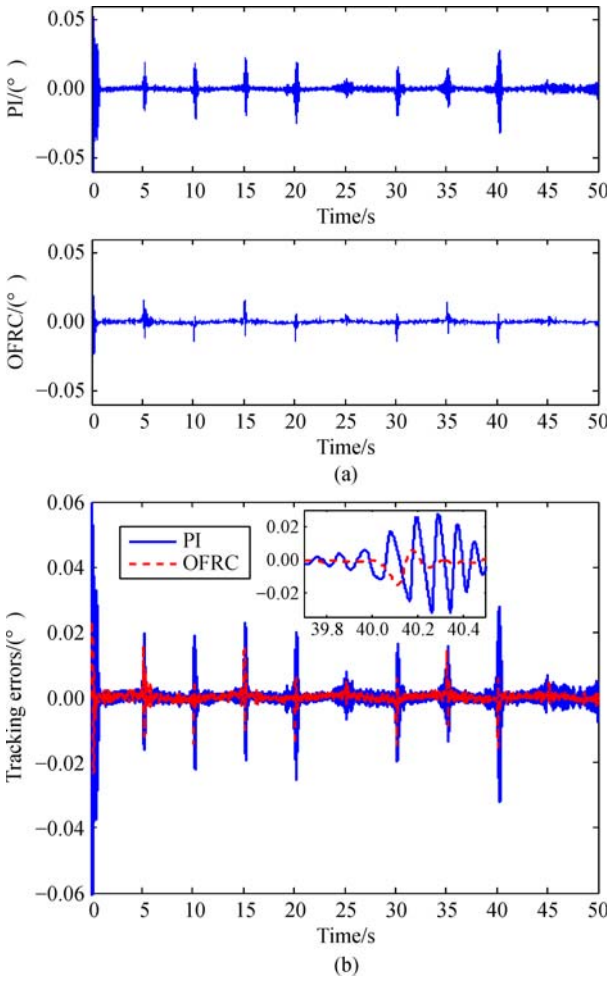

Fig. 20 Tracking errors of OFRC and PI controllers in slow tracking case. (a) Tracking errors during the whole period in slow tracking case; (b) comparison of tracking errors

Table 6 Performance indices in normal case

Indices	M_e	μ	σ
PI	0.0501	0.0097	0.0072
OFRC	0.0383	0.0517	0.0065

Table 7 Performance indices in slow tracking case

Indices	M_e	μ	σ
PI	0.0321	0.0019	0.0033
OFRC	0.0152	0.0008	0.0012

3.8.3 Experimental verification

For testing the effectiveness of the designed nonlinear output feedback controller (OFRC), it was experimentally compared with industrial PI controller in Ref. [28]. Firstly, the two controllers are tested for a sinusoidal-like motion trajectory $x_{1d} = 10[1-\cos(3.14t)][1-\exp(-t)]°$. The comparative tracking errors and the performance indices of the two controllers are shown in Fig. 19 and Table 6, respectively. To further verify the performance of the designed algorithm, a slow motion trajectory $x_{1d} = 10[1-\cos(0.628t)][1-\exp(-t)]°$ has been used. The tracking errors of the two controllers were depicted in Fig. 20. The performance indices for slow motion case were summarized in Table 7. Finally, to farthest consider the physical system existing complex working conditions and verify the robustness of the designed algorithm against to unmodeled disturbances, a fast motion trajectory $x_{1d} = 10[1-\cos(6.28t)][1-\exp(-t)]°$ is employed, meanwhile, a disturbance $0.3 + 0.02x_{1d}$ is added to the control input at $t = 10$ s through modifying the output function of D/A board, i.e., $u + 0.3 + 0.02x_{1d}$ is actually applied to the test rig after 10 s, in which u is calculated by OFRC/PI controller. In this fast motion case with disturbance, the PI controller was failed to handle such aggressive disturbance. Figure 21 gives the tracking error of OFRC

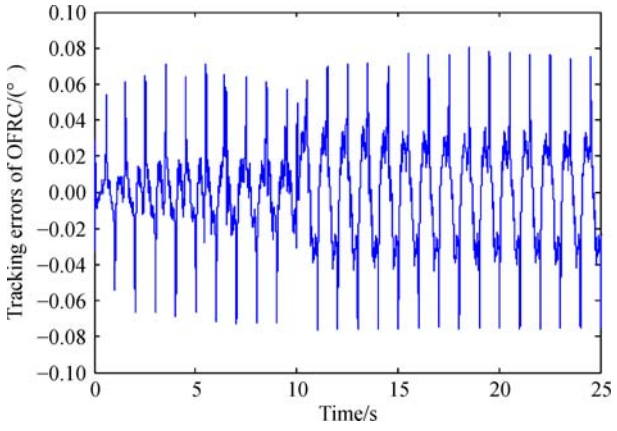

Fig. 21 Tracking errors of OFRC in fast tracking case with disturbance

controller. The following experimental results indicate that the designed nonlinear OFRC controller can obtain better tracking performance than the PI controller. For more details about the experiments, the reader is referred to Ref. [28].

3.9 State constraints control

The tracking control of hydraulic systems with constrained velocity and acceleration is taken into consideration in Case 9. To design the following adaptive backstepping control procedure with state constraints, the acceleration based state-space model in Eq. (13) and the modeled friction $f_r(t)$ in Eq. (3) are utilized for this case. In addition, it is assumed that the uncertain nonlinearities $f_e(t)$ and $q(t)$ are negligible. Thus, the system model for this case can be given as

$$\begin{cases} \dot{x}_1 = x_2 \\ \dot{x}_2 = x_3 \\ \dot{x}_3 = g_3(x,P_L)u - \dfrac{4\beta_e(A^2 + C_tB)}{mV_t}x_2 - \left(\dfrac{B}{m} + \dfrac{4\beta_e C_t}{V_t}\right)x_3, \\ \qquad -\dfrac{4\beta_e C_t A_f}{mV_t}S_f(x_2) - \dfrac{A_f}{m}\dot{S}_f(x_2) \end{cases} \tag{148}$$

where

$$g_3(x,P_L) \triangleq \frac{4A\beta_e k_t}{mV_t}\sqrt{P_s - \mathrm{sign}(u)P_L}. \tag{149}$$

Denote the unknown parameter set $\boldsymbol{\theta} = [\theta_1, \theta_2, \theta_3, \theta_4]^T$, where $\theta_1 = 4\beta_e(A^2 + C_tB)/m/V_t$, $\theta_2 = B/m + 4\beta_e C_t/V_t$, $\theta_3 = 4\beta_e C_t A_f/m/V_t$, $\theta_4 = A_f/m$, the system model in Eq. (148) can be written as

$$\begin{cases} \dot{x}_1 = x_2 \\ \dot{x}_2 = x_3 \\ \dot{x}_3 = g_3(x,P_L)u - \theta_1 x_2 - \theta_2 x_3 - \theta_3 S_f(x_2) - \theta_4 \dot{S}_f(x_2) \end{cases}. \tag{150}$$

In this section, the afore mentioned Assumptions 1, 2, and 3 are also needed, and the discontinuous projection mapping in Eq. (45) is also utilized.

Considering the magnitude constraints on the system velocity and acceleration result of physical performance limits or safety operation requirements as follows:

$$|x_2| \leqslant \Delta_v, |x_3| \leqslant \Delta_a, \tag{151}$$

where Δ_a and Δ_v denote the acceleration limitations and pre-set known velocity.

A Barrier Lyapunov function [29] is employed to prevent the system states from violating the constraints.

Definition 1. The scalar function $V(x)$ which is defined with respect to the system $\dot{x} = f(x)$ on an open region Θ containing the origin is a barrier Lyapunov function, and it is positive definite, continuous, has continuous first-order partial derivatives at every point of Θ, has the property $V(x) \to \infty$ as x approaches the boundary of Θ, and meets $V(x) \leqslant c$ (c is positive constant), $\forall t \geqslant 0$ along the solution of $\dot{x} = f(x)$ for $x(0) \in \Theta$.

3.9.1 Adaptive backstepping control design with velocity and acceleration constraints

Define the error variables as

$$z_1 = x_1 - x_{1d},\ z_2 = x_2 - \alpha_1,\ z_3 = x_3 - \alpha_2. \tag{152}$$

Define a function V_{s1} [30] as

$$V_{s1} = b_1 z_1 \mathrm{arctanz}_1, \tag{153}$$

where the designed constant gain $b_1 > 0$, the resulting control function α_1 is given by

$$\alpha_1 = x_{2d} - v_1 \mathrm{arctanz}_1, \tag{154}$$

where $v_1 > 0$. Then the function α_1 can be bounded by

$$|\alpha_1| < \frac{\pi}{2}v_1 + |x_{2d}|. \tag{155}$$

Then the time derivative of V_{s1} is

$$\dot{V}_{s1} = -\Xi_1 + b_1 z_2\left(\mathrm{arctanz}_1 + \frac{z_1}{1 + z_1^2}\right), \tag{156}$$

where

$$\Xi_1 = b_1 v_1 \mathrm{arctanz}_1\left(\mathrm{arctanz}_1 + \frac{z_1}{1 + z_1^2}\right). \tag{157}$$

Then, the following function candidate which comprises a barrier function is defined as

$$V_{s2}=V_{s1}+\frac{1}{2}b_2\log\frac{L_2^2}{L_2^2-z_2^2}. \tag{158}$$

The derivative of V_{s2} is given by

$$\dot{V}_{s2}=-\Xi_1+b_1z_2\left(\arctan z_1+\frac{z_1}{1+z_1^2}\right)+\frac{b_2z_2(x_3-\dot{\alpha}_1)}{L_2^2-z_2^2}, \tag{159}$$

which is a valid Lyapunov function during the internal $(-L_2,\ L_2)$ which represents the constraint on z_2, i.e., $|z_2|<L_2$. The resulting virtual control α_2 is given by

$$\alpha_2=\dot{\alpha}_1-v_2z_2-\frac{b_1}{b_2}(L_2^2-z_2^2)\left(\arctan z_1+\frac{z_1}{1+z_1^2}\right), \tag{160}$$

where the constant $v_2>0$, and

$$\dot{\alpha}_1=x_{3d}-\frac{v_1\dot{z}_1}{1+z_1^2}. \tag{161}$$

Based on Eq. (159), it can be obtained

$$\dot{V}_2=-\Xi_2+\frac{b_2z_2z_3}{L_2^2-z_2^2}, \tag{162}$$

where

$$\Xi_2=\Xi_1+\frac{b_2v_2z_2^2}{L_2^2-z_2^2}. \tag{163}$$

Denote the following function V_{s3} as

$$V_{s3}=V_{s2}+\frac{1}{2}b_3\log\frac{L_3^2}{L_3^2-z_3^2}+\frac{1}{2}\tilde{\boldsymbol{\theta}}^{\mathrm{T}}\boldsymbol{\Gamma}^{-1}\tilde{\boldsymbol{\theta}}, \tag{164}$$

where $b_3>0$.

It is easy to check that V_{s3} is a valid Lyapunov function during the internal $(-L_3,\ L_3)$ which represents the constraint on z_3, i.e., $|z_3|<L_3$. The time derivative of V_{s3} is

$$\dot{V}_{s3}=\dot{V}_{s2}+b_3\frac{z_3\dot{z}_3}{L_3^2-z_3^2}=-\Xi_2+\frac{b_2z_2z_3}{L_2^2-z_2^2}+b_3\frac{z_3\left[g_3u-\theta_1x_2-\theta_2x_3-\theta_3S_f-\theta_4\dot{S}_f-\dot{\alpha}_2\right]}{L_3^2-z_3^2}+\tilde{\boldsymbol{\theta}}^{\mathrm{T}}\boldsymbol{\Gamma}^{-1}\dot{\hat{\boldsymbol{\theta}}}, \tag{165}$$

where $\dot{\alpha}_2$ is given by

$$\dot{\alpha}_2=\dot{x}_{3d}-\frac{v_1\ddot{z}_1}{1+z_1^2}+\frac{2v_1z_1\dot{z}_1^2}{(1+z_1^2)^2}-v_2\dot{z}_2+\frac{2b_1}{b_2}z_2\dot{z}_2\left(\arctan z_1+\frac{z_1}{1+z_1^2}\right)-\frac{b_1}{b_2}\frac{2\dot{z}_1}{1+z_1^2}\times(L_2^2-z_2^2)\left(1-\frac{z_1^2}{1+z_1^2}\right). \tag{166}$$

Then design the control input as

$$u=\frac{1}{g_3}\left[\hat{\theta}_1x_2+\hat{\theta}_1x_3+\hat{\theta}_3S_f+\hat{\theta}_4\dot{S}_f+\dot{\alpha}_2-\frac{b_2}{b_3}\frac{L_3^2-z_3^2}{L_2^2-z_2^2}z_2-v_3z_3\right], \tag{167}$$

where $v_3>0$ and the adaptation law $\boldsymbol{\tau}$ as

$$\boldsymbol{\tau}=\boldsymbol{\varphi}z_3, \tag{168}$$

in which

$$\boldsymbol{\varphi}=\left[-\frac{b_3x_3}{L_3^2-z_3^2},-\frac{b_3\dot{S}_f(x_2)}{L_3^2-z_3^2}\right]^{\mathrm{T}}.$$

Substituting Eqs. (167) and (168) into Eq. (165),

$$\dot{V}_{s3}=-\Xi_2-\frac{b_3v_2z_3^2}{L_3^2-z_3^2}=-\Xi_3, \tag{169}$$

where

$$\Xi_3=\Xi_2+\frac{b_3v_2z_3^2}{L_3^2-z_3^2}, \tag{170}$$

is positive-definite and $\boldsymbol{z}$ is defined as $\boldsymbol{z}=[z_1,\ z_2,\ z_3]^{\mathrm{T}}$. Then the system acceleration x_3 is bounded as z_3 and α_2 are bounded.

3.9.2 Stability analysis

Theorem 9: If the initial conditions satisfy $\boldsymbol{z}(0)\in\boldsymbol{\Omega}_{z0}$: $\{\boldsymbol{z}(0)\in R^3:\ |z_2(0)|<L_2,\ |z_3(0)|<L_3\}$, with the designed projection type adaptation law Eq. (46) and adaptation function Eq. (168), the devised controller Eq. (167) can guarantee:

A. All closed loop signals in the system are bounded. And the tracking errors z_2 and z_3 are bounded by

$$\begin{cases} z_2 < L_2\sqrt{1-\mathrm{e}^{-2V_{s3}(0)/b_2}} \\ z_3 < L_3\sqrt{1-\mathrm{e}^{-2V_{s3}(0)/b_3}} \end{cases}. \tag{171}$$

B. Not only the results in A are obtained, but also the asymptotic output tracking is achieved, i.e., $z_1\to 0$ as $t\to\infty$.

Proof: From Eq. (169), $\dot{V}_{s3}\leqslant 0$, it can be obtained that $V_{s3}(t)$ is bounded, which provides that $V_{s3}(0)$ is a non-increasing function and is bounded. Then $V_{s1}(t)$ and $V_{s2}(t)$ are bounded. Thus, $|z_2(t)|<L_2$, $|z_3(t)|<L_3$. Then it can be inferred that

$$\begin{cases} \frac{1}{2}b_2\log\frac{L_2^2}{L_2^2-z_2^2}\leqslant V_{s2}\leqslant V_{s3}\leqslant V_{s3}(0) \\ \frac{1}{2}b_3\log\frac{L_3^2}{L_3^2-z_3^2}\leqslant V_{s2}\leqslant V_{s3}\leqslant V_{s3}(0) \end{cases}. \tag{172}$$

Thus, through rearranging and taking exponentials on both sides of the inequality Eq. (172), Eq. (171) can be obtained. For the situation in B of Theorem 1, by Barbalat's lemma, $\Xi_3 \to 0$ as $t \to \infty$, it leads to B of Theorem 9 from Eq. (170).

3.9.3 Simulation verification

To test the effectiveness of the developed adaptive backstepping controller (ABC) with velocity and acceleration constraints, simulation results were obtained by comparing the ABC controller with the robust adaptive controller (RAC). In the simulation, to verify how the initial conditions affect the violation of system constraints, it is fixed that $z_1(0) = -1$, $z_2(0) = 0$ and $z_3(0) = 0$. In addition, the constraints of acceleration and velocity are pre-set as $\Delta_a = 100$ m/s^2 and $\Delta_v = 5$ m/s. To make the tracking error as small as possible while respecting the system constraints is the control objective. Figure 22 shows the comparative tracking performance of the two controllers. The velocity and acceleration output under the two controllers are given in Figs. 23 and 24, respectively. The simulation results show that the developed ABC obtains small tracking error, same as RAC, except the start transient period, and ensures that the velocity and acceleration constraints have never been violated. More details of this simulation can be found in Ref. [31].

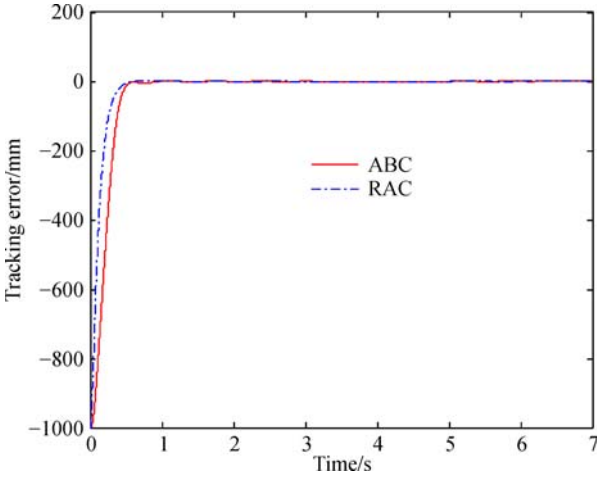

Fig. 22 Tracking errors with $z_1(0) = -1$

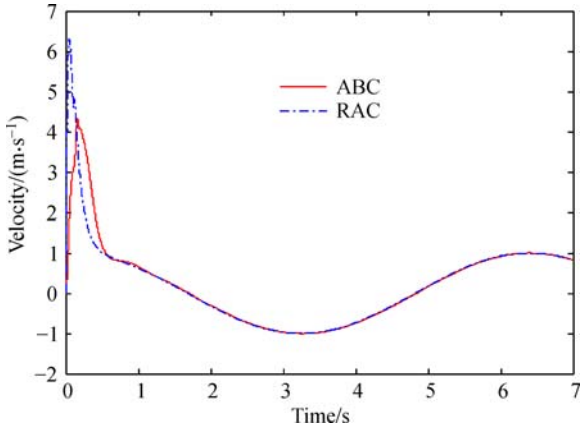

Fig. 23 Velocity output with $z_1(0) = -1$

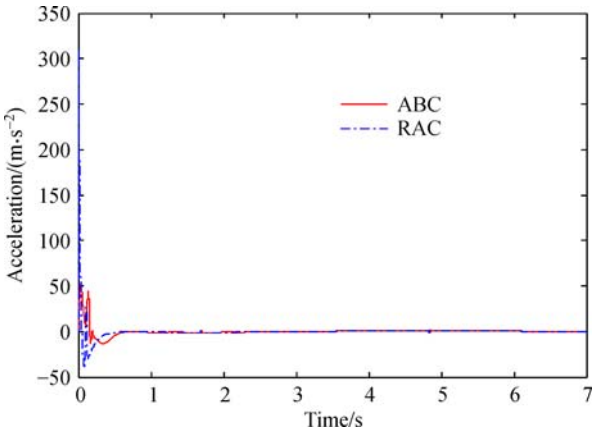

Fig. 24 Acceleration output with $z_1(0) = -1$

4 Perspectives for opening problems

Although the proposed methods above can solve most tracking problems of hydraulic servo systems, there are still some opening problems remain unsolved, as discussed bellow.

4.1 Enhanced adaptive control with disturbance observer

As presented in adaptive robust control for hydraulic systems, the developed ARC controller can guarantee a prescribed transient tracking performance and final tracking accuracy as well as asymptotic output tracking with parametric uncertainties only. However, high-gain feedback issue also lies in ARC since large feedback gains have to be used to speed up the transient response and reduce the final tracking error when hydraulic servo systems are subjected to large uncertain nonlinearities. It is known that disturbance observer based control has also been extensively researched to cope with large modelling uncertainties. As shown in LESO design in output feedback control for hydraulic systems, the ESO can estimate the generalized disturbances and compensate them in a feedforward way, and the uncertainty estimation error can be made small enough by increasing the observer bandwidth. However, the parameterizable uncertainties are not considered explicitly in ESO-based design, which increases the learning burden of ESO. Consequently, compared with adaptive control, ESO-based design would perform worse tracking performance for systems subjected to heavy parametric uncertainties.

Hence, how to develop an advanced nonlinear controller

for hydraulic systems to handle both heavy parametric uncertainty and uncertain nonlinearity is still an opening problem. An instinct thought is that if adaptive control and ESO can be merged via full state feedback into one controller in which parametric uncertainties and uncertain nonlinearities are handled separately, then improved tracking performance can be expected. However, their fundamentally working mechanisms are totally different, how to integrate these two control methods that can preserve the advantages of both design approaches, while getting over their practical performance limitations should be given special attention.

4.2 Servo-valve input nonlinearity

The most nonlinear models for hydraulic systems assume the servo valve is ideal, as like in Eqs. (5) and (10). This assumption ignores any effects in servo valve, and directly applies proportional relationship between the final control input u and the valve spool position x_v. However, any actual valve contains some nonlinearities which typically include input saturation, dead-zone, and hysteresis, etc. These input nonlinearities may cause the controlled hydraulic system to be unstable or present bad tracking performance.

Input saturation is the most common nonlinearity in control systems. The saturation in hydraulic system may be caused by maximum velocity/force/power requirements. At any case, during the saturation period, the hydraulic system is uncontrollable. In general, there are two ways to handle saturation problem: One is to make the controller naturally possess the property that at any case, the controller output will never exceed one pre-set value, i.e., the saturation will never happen no matter the maximum velocity/force/power requirements. The major technique point in this design concept is: The trajectory is first planned that the saturation cannot be caused by demands, and the second is to make the feedback go into the controller via saturation projections which can ensure that the feedback control actions result in a bounded control value no matter how large the tracking errors are. Actually, this design concept is rather conservative, and the design difficulty of this concept is how to cope with various modelling uncertainty to result in a balanced control input that as just perfectly as possible controls the system to satisfy the demands and against various uncertainties. The other way is to permit the occurrence of input saturation, however, design a saturation compensator which will be activated at the saturation point, and the mission of this compensator is to ensure the closed-loop stability during saturation while ideally restore the previous control performance when the cause of saturation disappears. The difficult lying in the second saturation approach is the compensator design and the stability analysis of the closed-loop system.

Dead-zone nonlinearity typically results from coulomb friction and from overlap of valve ports in hydraulic systems, and is a critical issue for high-accuracy tracking control of hydraulic servo systems, especially in proportional control fields driven by proportional valves. Inappropriate action for dead-zone nonlinearity may cause limit cycles. Hence suitable dead-zone compensation technique possesses many practical meanings. To alleviate the effect of dead-zone, there are generally two kinds of ways in the literature. One is inverse function based adaptive control. It is worth noting that most constructed dead-zone inverses are discontinuous, which may cause the control input chattering. Hence, a smooth dead-zone inverse will be more popular for hydraulic systems, as shown in Fig. 25. However, almost all active dead-zone compensation based controllers can ensure the convergence of the tracking error goes to a residual bounded set only. The other way of eliminating the dead-zone effect is to see the dead-zone as a time-varying disturbance-like term. With this formulation, various robust feedback control laws have been used to handle the disturbance-like term. However, by treating the dead-zone as a disturbance-like term if nonlinear system is subjected to sever dead-zone may cause high gain feedback issue, i.e., large slopes or breakpoints. Hence, there is an imperative pursuit for active smooth dead-zone compensation with the enhanced robust feedback mechanism to further improve the tracking performance of hydraulic systems, eliminate potential instability caused by dead-zone.

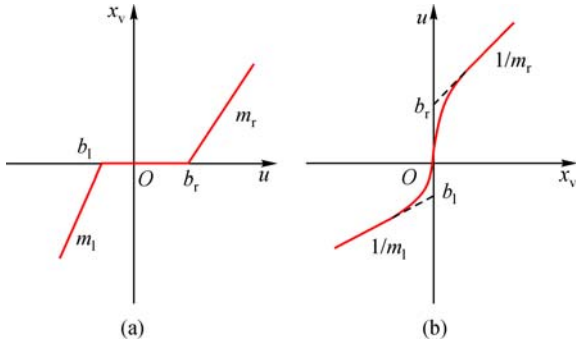

Fig. 25 Dead-zone effects and its smooth inverse

Unlike the above discussed single-valued nonlinearities, magnetic components, such as electric servomotors of direct-driven valve and torque motors of nozzle flapper servo valve, commonly have a multi-valued nonlinear characteristic, i.e., hysteresis, as shown below in Fig. 26. The input of this figure is the control voltage, and the output of this figure is the applied voltage through the hysteresis effect. The width of the hysteresis loop varies directly with the input signal. Based on linear analysis, it is known that the hysteresis nonlinearity is not a serious threat to stability. However, the most adverse property of hysteresis is a fixed amount of phase lag at low frequencies. Typically, this phase lag can be ignored

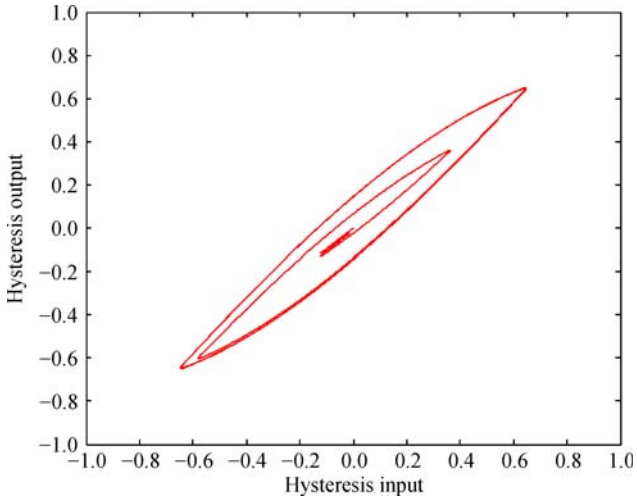

Fig. 26 Multi-valued effects of an example of hysteresis

since the it is very small, meanwhile the hysteresis effects are very small in nozzle flapper servo valves. However, it should be noticeable when ultra-high accuracy tracking performance is required, or as fashionable currently, when proportional valves or proportional servo-valves are utilized, the active compensation for hysteresis should be paid more attention. Effective hysteresis models for model-based nonlinear control, and the uncertainty handling mechanisms associated with hysteresis are still opening problems for high performance hydraulic servo control system.

4.3 High dynamic control

Bandwidth is a meaningful, useful and powerful concept for control engineering, resulted from frequency domain design and analysis. As it is well known that this concept is founded on the linear control theory and only suitable for linear systems. However, nonlinear control methods for hydraulic systems are time-domain based design and analysis, there is no frequency concept. Hence, a valuable proposition is that is it possible to deduce a frequency bandwidth or develop a series tools to reflect the frequency bandwidth for nonlinear controllers. To the author's opinion, the frequency concept is able to be discussed for nonlinear control at least. This statement arises another problem for nonlinear hydraulic servo control, i.e., the high dynamic control. To the best of our knowledge, the existing nonlinear methods verified by experiments only related low frequency tracking performance. The high frequency tracking experimental results are very little. The theoretical results from nonlinear control methods also puzzle people that their stability is irrelevant with frequency, and the mathematical proof is rigorous. Does this mean that the nonlinear controller can track any high frequency trajectories? It seems correct to theorists, however incorrect to practitioners. There is a huge gap between theory and practice. That is to say, the tracking performance will be what if continually increasing the frequency of the desired trajectory.

In addition, at high frequency tracking stage, the valve dynamics can be ignored any more, i.e., the dynamic effects between the final control input and the spool position of servo valve cannot be simplified by proportional relationship. How considering the valve dynamics to design nonlinear backstepping controllers for hydraulic systems is a challenging issue result of the differential explosion with backstepping if directly involving the valve dynamics as first or second order differential equations. Besides the valve dynamics, the mechanical stiffness effects may be not ignored either at high frequency tracking stage. Relying on different sensors layout, the mechanical stiffness affects the system via inner-loop effects or outer loop effects. How designing suitable nonlinear controllers to actively compensate or passively robust against these stiffness effects is an opening problem.

4.4 Noise alleviation

In almost all nonlinear control strategies for hydraulic systems, the effects of measurement noise accompanied in full state feedback are not specifically taken into consideration. Practice reveals that measurement noise has become the core problem in achieving high tracking performance in some cases. For electro-hydraulic servo systems, the noise mainly comes from the measurement of velocity and pressure signals. Almost all nonlinear controllers are based on the noise-free theoretical design, while via various low-pass filters to alleviate noise effects in practice. However, filters are not considered in the design stage and will cause severe phase lag in high frequency range.

To alleviate the noise effects, there are generally three kinds of methods in the literature. The first is the dynamic surface control (DSC) based schemes which can solve the problem of "explosion of complexity" in the backstepping design and avoid the feedback signal noise amplification result of repeated differentiations of virtual controllers through introducing a first-order filtering of the synthesized virtual control law at each backstepping design procedure. However, the full state feedback DSC schemes can do nothing about the noisy states contained in the final control law. Moreover, the phase lag issue caused by the low-pass filters also lies in the DSC schemes. The second is the output feedback control approach which only utilizes the output measurement while the noise contaminated velocity and pressure states are estimated by various state observers. However, observer based nonlinear control strategies suffer from the learning capability of the utilized observer, and encounter bad performance during the transient period of the observer and heavy parametric uncertainties. Another good alternative way of attenuating the effect of measurement noise is the desired compensa-

tion adaptive control which was first introduced by Sadegh and Horowitz [32]. An excellent benefit is that desired compensation can be easily integrated with adaptive and robust control by constructing noise-free desired values to replace noisy actual states, and hence possesses strong capability to suppress various uncertainties. However, for uncertain nonlinear systems with unmatched modeling uncertainties and input nonlinearities, such as hydraulic systems, the desired values of the intermediate state variables cannot be predetermined based on the common way as in Ref. [32]. Additionally, hydraulic system should be thought as non-affine system due to the existence of control input dependent nonlinear function, which further complicates the design of adaptive desired compensation controller. Typically, developing a desired value for velocity state is not difficult, however, for pressure information is still a pending problem.

5 Conclusions

In this paper, the author expressed his viewpoints on hydraulic nonlinear modelling methods, control challenges, recent developments to handle various modelling uncertainties for model-based nonlinear control of hydraulic servo systems. Although various advanced nonlinear control methods have been proposed, there are still lots of opening problems associated with hydraulic nonlinear control, such as further enhanced adaptive control with disturbance observer to both handle heavy parametric uncertainty and uncertain nonlinearity, input nonlinearity control, high dynamic control, noise alleviation methods for practical hydraulic systems. This paper hopes to initiate other decent and creative inspirations to promote the development of nonlinear control technology for electro hydraulic servo systems.

Acknowledgements This work was supported in part by the National Natural Science Foundation of China (Grant No. 51675279), the China Postdoctoral Science Foundation funded project (Grant Nos. 2014M551593 and 2015T80553), and the Natural Science Foundation of Jiangsu Province in China (Grant No. BK20141402). The author also wants to express his appreciation to Prof. B. Yao for hosting his visit at Purdue University from October 2010 to October 2011, and the guidance in adaptive and robust design.

References

1. Merritt H E. Hydraulic Control Systems. New York: Wiley, 1967
2. Yao B, Bu F, Reedy J, et al. Adaptive robust motion control of single-rod hydraulic actuators: Theory and experiments. IEEE/ASME Transactions on Mechatronics, 2000, 5(1): 79–91
3. Krstic M, Kanellakopoulos I, Kokotovic P V. Nonlinear and Adaptive Control Design. New York: Wiley, 1995
4. Armstrong-Hélouvry B, Dupont P, Canudas de Wit C. A survey of models, analysis tools and compensation methods for the control of machines with friction. Automatica, 1994, 30(7): 1083–1138
5. Canudas de Wit C, Olsson H, Astrom K J, et al. A new model for control of systems with friction. IEEE Transactions on Automatic Control, 1995, 40(3): 419–425
6. Swevers J, Al-Bender F, Ganseman C G, et al. An integrated friction model structure with improved presliding behavior for accurate friction compensation. IEEE Transactions on Automatic Control, 2000, 45(4): 675–686
7. Yao J, Jiao Z, Ma D, et al. High-accuracy tracking control of hydraulic rotary actuators with modelling uncertainties. IEEE/ASME Transactions on Mechatronics, 2014, 19(2): 633–641
8. Yao J, Deng W, Jiao Z. RISE-based adaptive control of hydraulic systems with asymptotic tracking. IEEE Transactions on Automation Science and Engineering, 2017, 14(3): 1524–1531
9. Lischinsky P, Canudas de Wit C, Morel G. Friction compensation for an industrial hydraulic robot. IEEE Control Systems Magazine, 1999, 19 (1): 25–32
10. Swaroop D, Hedrick J K, Yip P P, et al. Dynamic surface control for a class of nonlinear systems. IEEE Transactions on Automatic Control, 2000, 45(10): 1893–1899
11. Yip P P, Hedrick J K. Adaptive dynamic surface control: A simplified algorithm for adaptive backstepping control of nonlinear systems. International Journal of Control, 1998, 71(5): 959–979
12. Farrell J A, Polycarpou M, Sharma M, et al. Command filtered backstepping. IEEE Transactions on Automatic Control, 2009, 54 (6): 1391–1395
13. Dong W, Farrell J A, Polycarpou M M, et al. Command filtered adaptive backstepping. IEEE Transactions on Control Systems Technology, 2012, 20(3): 566–580
14. Guan C, Pan S. Adaptive sliding mode control of electro-hydraulic system with nonlinear unknown parameters. Control Engineering Practice, 2008, 16(11): 1275–1284
15. Guan C, Pan S. Nonlinear adaptive robust control of single-rod electro-hydraulic actuator with unknown nonlinear parameters. IEEE Transactions on Control Systems Technology, 2008, 16(3): 434–445
16. Mintsa H A, Venugopal R, Kenne J P, et al. Feedback linearization-based position control of an electrohydraulic servo system with supply pressure uncertainty. IEEE Transactions on Control Systems Technology, 2012, 20(4): 1092–1099
17. Yao J, Yang G, Jiao Z. High dynamic feedback linearization control of hydraulic actuators with backstepping. Proceedings of the Institution of Mechanical Engineers, Part I: Journal of Systems and Control Engineering, 2015, 229: 728–737
18. Yao J, Jiao Z, Yao B, et al. Nonlinear adaptive robust force control of hydraulic load simulator. Chinese Journal of Aeronautics, 2012, 25 (5): 766–775
19. Yang G, Yao J, Le G, et al. Adaptive integral robust control of hydraulic systems with asymptotic tracking. Mechatronics, 2016, 40: 78–86
20. Deng W, Yao J. Adaptive integral robust control and application to electromechanical servo systems. ISA Transactions, 2017, 67: 256–265
21. Yang G, Yao J, Le G, et al. Asymptotic output tracking control of electro-hydraulic systems with unmatched disturbances. IET Control Theory & Applications, 2016, 10(18): 2543–2551

22. Yao B, Xu L. On the design of adaptive robust repetitive controllers. In: Proceedings of 2001 ASME International Mechanical Engineering Congress and Exposition. New York: ASME, 2001, 1–9
23. Yao J, Jiao Z, Ma D. A practical nonlinear adaptive control of hydraulic servomechanisms with periodic-like disturbances. IEEE/ASME Transactions on Mechatronics, 2015, 20(6): 2752–2760
24. Yao J, Deng W, Jiao Z. Adaptive control of hydraulic actuators with LuGre model based friction compensation. IEEE Transactions on Industrial Electronics, 2015, 62(10): 6469–6477
25. Xu L, Yao B. Adaptive robust control of mechanical systems with nonlinear dynamic friction compensation. International Journal of Control, 2008, 81(2): 167–176
26. Tan Y, Kanellakopoulos I. Adaptive nonlinear friction compensation with parametric uncertainties. In: Proceedings of the 1999 American Control Conference. San Diego: IEEE, 1999, 2511–2515
27. Zheng Q, Gao L, Gao Z. On stability analysis of active disturbance rejection control for nonlinear time-varying plants with unknown dynamics. In: Proceedings of 2007 46th IEEE Conference on Decision and Control. New Orleans: IEEE, 2007, 3501–3506
28. Yao J, Jiao Z, Ma D. Extended-state-observer-based output feedback nonlinear robust control of hydraulic systems with backstepping. IEEE Transactions on Industrial Electronics, 2014, 61(11): 6285–6293
29. Tee K P, Ge S S, Tay E H. Barrier Lyapunov function for the control of output-constrained nonlinear systems. Automatica, 2009, 45(4): 918–927
30. Ngo K B, Mahony R, Jiang Z P. Integrator backstepping using barrier functions for systems with multiple state constraints. In: Proceedings of 44th IEEE Conference on Decision and Control, and 2005 European Control Conference. Seville: IEEE, 2005, 8306–8312
31. Deng W, Yao J, Jiao Z. Adaptive backstepping motion control of hydraulic actuators with velocity and acceleration constraints. In: Proceedings of 2014 IEEE Chinese Guidance, Navigation and Control Conference (CGNCC). Yantai: IEEE, 2014, 219–224
32. Sadegh N, Horowitz R. Stability and robustness analysis of a class of adaptive controllers for robot manipulators. International Journal of Robotics Research, 1990, 9(3): 74–92